Cysteine accessibility probes timing and extent of NBD separation along the dimer interface in gating CFTR channels

Luiz A. Poletto Chaves and David C. Gadsby

The Laboratory of Cardiac/Membrane Physiology, The Rockefeller University, New York, NY 10065

Cystic fibrosis transmembrane conductance regulator (CFTR) channel opening and closing are driven by cycles of adenosine triphosphate (ATP) binding–induced formation and hydrolysis-triggered disruption of a heterodimer of its cytoplasmic nucleotide-binding domains (NBDs). Although both composite sites enclosed within the heterodimer interface contain ATP in an open CFTR channel, ATP hydrolysis in the sole catalytically competent site causes channel closure. Opening of the NBD interface at that site then allows ADP–ATP exchange. But how frequently, and how far, the NBD surfaces separate at the other, inactive composite site remains unclear. We assessed separation at each composite site by monitoring access of nucleotide-sized hydrophilic, thiol-specific methanothiosulfonate (MTS) reagents to interfacial target cysteines introduced into either LSGGQ-like ATP-binding cassette signature sequence (replacing equivalent conserved serines: S549 and S1347). Covalent MTS-dependent modification of either cysteine while channels were kept closed by the absence of ATP impaired subsequent opening upon ATP readdition. Modification while channels were opening and closing in the presence of ATP caused macroscopic CFTR current to decline at the same speed as when the unmodified channels shut upon sudden ATP withdrawal. These results suggest that the target cysteines can be modified only in closed channels; that after modification the attached MTS adduct interferes with ATP-mediated opening; and that modification in the presence of ATP occurs rapidly once channels close, before they can reopen. This interpretation was corroborated by the finding that, for either cysteine target, the addition of the hydrolysis-impairing mutation K1250R (catalytic site Walker A Lys) similarly slowed, by an order of magnitude, channel closing on ATP removal and the speed of modification by MTS reagent in ATP. We conclude that, in every CFTR channel gating cycle, the NBD dimer interface separates simultaneously at both composite sites sufficiently to allow MTS reagents to access both signature-sequence serines. Relatively rapid modification of S1347C channels by larger reagents—MTS-glucose, MTS-biotin, and MTS-rhodamine—demonstrates that, at the noncatalytic composite site, this separation must exceed 8 Å.

INTRODUCTION

ATP-binding cassette (ABC) proteins are multidomain ATPases that form a superfamily represented in all kingdoms of life (Davidson et al., 2008). Their integral ATPase motor comprises a pair of cytoplasmic ABCs, also called nucleotide-binding domains (NBDs), for which there are >350,000 sequences (Pfam database accession no. PF00005; http://pfam.sanger.ac.uk/family/ABC_tran). Structural and functional analyses have established that these NBDs form head-to-tail dimers enclosing two composite interfacial catalytic sites for ATP binding and hydrolysis (e.g., Hopfner et al., 2000; Smith et al., 2002). ATP binding leads to dimerization of the NBDs, and hydrolysis of bound ATP causes their separation (Moody et al., 2002; Verdon et al., 2003). The relative NBD motions are transmitted through coupling helices to specific effector domains to carry out a range of tasks; some ABC proteins repair DNA (Hopfner and Tainer, 2003; Lamers et al., 2003) and some regulate ribosomes (Boël et al., 2014), but most are membrane proteins that function as transporters (Davidson et al., 2008; Rees et al., 2009). In ABC transporters, the NBD movements drive conformational changes of attached transmembrane domains, between outward-facing and inward-facing states that alternately open the substrate binding pocket to one or other side of the plasma membrane.

Accumulated functional and structural information has clarified the mechanistic underpinnings of ABC transporter catalytic cycles. Most structural detail has come from homodimeric bacterial transporters, or isolated NBDs, in which the two composite ATP sites are identical. Present evidence suggests that in homodimers, the ATP hydrolysis mechanism is the same in both catalytic sites, and the same in ABC importers (e.g., Oldham and Chen, 2011b) as in exporters (e.g., Smith et al., 2002), in accord with strict conservation of the key NBD sequence motifs. In ATP-bound tight NBD homodimers, each nucleotide contacts Walker A and B

Correspondence to David C. Gadsby: gadsby@rockefeller.edu

Abbreviations used in this paper: ABC, ATP-binding cassette; MTSACE, 2-aminocarbonyl-ethyl-MTS; $MTSES^-$, 2-sulfonato-ethyl-MTS; $MTSET^+$, 2-trimethylammonium-ethyl-MTS; NBD, nucleotide-binding domain; NEM, *N*-ethylmaleimide.

The Rockefeller University Press $30.00
J. Gen. Physiol. Vol. 145 No. 4 261–283
www.jgp.org/cgi/doi/10.1085/jgp.201411347

sequences in the head of one NBD and the ABC signature sequence, LSGGQ, in the other NBD tail (Fig. 1 F). The Walker A motif, or P loop (Fig. 1, red), curves around, and positions, the ATP phosphate chain; the glutamate immediately following the Walker B hydrophobic residues is the catalytic base that polarizes the attacking water molecule; and the signature sequence (Fig. 1, purple) serine and second glycine both contact the γ phosphate (Hung et al., 1998; Moody et al., 2002; Smith et al., 2002; Chen et al., 2003; Verdon et al., 2003; Dawson and Locher, 2006; Oldham and Chen, 2011b).

The most complete structural cycle has been determined for the bacterial maltose importer, MalEFGK2 (Khare et al., 2009; Oldham and Chen, 2011a), whereas that of ABC exporters, more closely related to human ABC proteins, is less complete. The highest resolution crystal structures of homodimeric prokaryotic exporters were initially outward-facing conformations, with the transmembrane pathway open to the periplasm and tightly dimerized nucleotide-bound NBDs; these include the multidrug transporter homologues Sav1866, with bound ADP (Dawson and Locher, 2006) or poorly hydrolyzable ATP analogue AMPPNP (Fig. 1 C; Dawson and Locher, 2007), and MsbA with bound AMPPNP (Ward et al., 2007). But recent high resolution structures have captured inward-facing conformations of exporters, both prokaryotic and eukaryotic, including homodimeric half-transporters and full-length transporters, most obtained in the absence of nucleotides. These apo structures have displayed a range of NBD separations, far apart in some cases, e.g., >50 Å in one form of MsbA (Ward et al., 2007), and up to 35 Å in three different P-gp crystals (Aller et al., 2009; Jin et al., 2012; Li et al., 2014), but closer together in other cases, e.g., ∼13 Å in ABCB1 from a red alga (Kodan et al., 2014), ∼8 Å in human mitochondrial ABCB10 (Shintre et al., 2013),

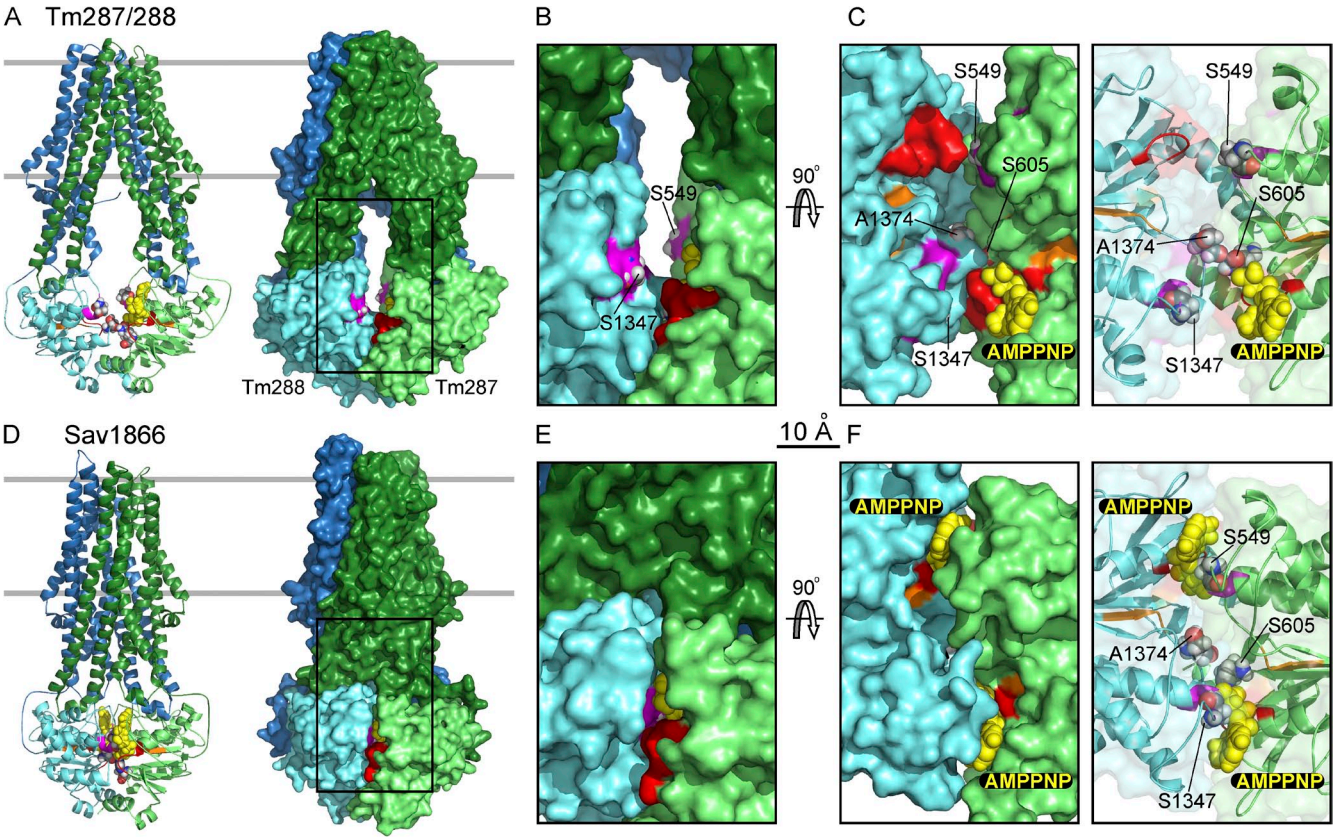

Figure 1. Structural comparison of heterodimeric, TM287/288 (A–C), and homodimeric, Sav1866 (D–F), ABC transporters. (A and D) Cartoon (left) and surface (right) representations of TM287/288 (A; PDB accession no. 3QF4) and Sav1866 (D; PDB accession no. 2ONJ) viewed along expected membrane plane (boundaries indicated by gray lines). Transmembrane domains equivalent to CFTR's transmembrane domain 1 and transmembrane domain 2 are forest green and blue, respectively; NBDs equivalent to CFTR's NBD1 and NBD2 are lime and cyan, respectively. Walker A motifs are shown in red, Walker B in orange, ABC signature in purple, bound AMPPNP as yellow spheres, and target residue positions as CPK spheres. (B and E) Magnified (∼2×) surface views of the boxed cytoplasmic regions in A and D. Interfacial residues equivalent to CFTR's ABC signature-sequence targets S549 and S1347 are exposed in TM287/288 (B) but buried in Sav1866 (E). (C and F) NBD dimer interfaces viewed from the membrane, after 90° rotation from B and E views and removal of transmembrane domains, with solid (left) and transparent (right) surfaces. In Sav1866 (F), a signature sequence and AMPPNP are buried in the tight NBD dimer interface in each composite site, whereas in TM287/288 (C), both signature sequences are exposed and a single AMPPNP is bound by the CFTR equivalent NBD1 Walker A motif.

and ∼4 Å in an alternate form of MsbA (Ward et al., 2007). Remarkably, even ABCB10 crystallized in AMPPNP or AMPPCP was found to adopt inward-facing conformations, with nucleotide-bound NBDs still separated by roughly 10 Å (Shintre et al., 2013).

Less structural information is available for the group of inherently asymmetric ABC proteins in which evolution has rendered one of the composite interfacial ATP-binding sites noncatalytic. Human ABC subfamily C members epitomize this class and include CFTR (ABCC7), the sulfonylurea receptors SUR1 and SUR2 (ABCC8 and ABCC9) that regulate potassium channels, and the multidrug resistance–related protein MRP1 (ABCC1) that exports cytotoxic drugs. Similarly, asymmetric NBDs are found in the subfamily B transporters associated with antigen processing, TAP1 and TAP2 (ABCB2 and ABCB3). Biochemical evidence has shown that ATP hydrolysis occurs exclusively in the NBD2 composite site (comprising NBD2 head Walker motifs and NBD1 tail LSGGQ signature motif) but that ATP remains bound at the NBD1 composite site (NBD1 head and NBD2 tail) without being hydrolyzed, for long periods compared with the catalytic cycle time, in SUR1 (Matsuo et al., 1999), MRP1 (Gao et al., 2000; Hou et al., 2000; Nagata et al., 2000), CFTR (Aleksandrov et al., 2002; Basso et al., 2003), and TAP1/TAP2 (Procko et al., 2006). Comparable asymmetric function has been demonstrated for the heterodimeric prokaryotic drug transporters LmrCD (Lubelski et al., 2006) and TmrAB (Zutz et al., 2011). For these asymmetric ABC proteins, therefore, hydrolysis of a single ATP must suffice for a complete conformational cycle, raising the question of whether NBD separation might also be asymmetric, occurring predominantly at the catalytic site to allow release of the hydrolysis product, ADP. However, two recent structures of the asymmetric ABC transporter, TM287/288 from the thermophilic prokaryote *Thermotoga maritima*, one crystallized in the presence of AMPPNP (Fig. 1; Hohl et al., 2012) and the other in the absence of nucleotide (Hohl et al., 2014), both reveal inward-facing conformations of the transmembrane domains with the NBDs separated by ∼10 Å at both composite sites, despite the presence of a single AMPPNP bound to Walker motifs of the "NBD1" head (TM287) in one structure (Fig. 1; Hohl et al., 2012). The NBDs are also ∼10 Å apart in a new single-particle cryo-EM structure of apo TmrAB, but in a surprisingly symmetrical arrangement in which disruption of both composite sites by lateral sliding brings the Walker A motifs opposite each other across the dimer interface (Kim et al., 2015). But little functional information exists about the location, timing, and distance of NBD separation, for comparison with this structural information.

CFTR is an exemplar asymmetric ABC protein, and CFTR channel chloride ion currents have provided a window into the coupling between the catalytic cycle of the NBDs and conformational changes in the transmembrane ion pathway, with single molecule and single cycle resolution. A CFTR channel opens after two ATPs bind and cause tight NBD1–NBD2 heterodimerization, which switches the transmembrane domains to an outward-facing open anion pore conformation; phosphate loss after ATP hydrolysis at the active "NBD2" composite site prompts heterodimer dissociation, which restores the inward-facing conformation of the transmembrane domains, closing the ion channel, whereupon exchange of ATP for ADP at the active site starts the next cycle (Gadsby et al., 2006; Chen and Hwang, 2008; see also Csanády et al., 2010). The ATP that remains in the catalytically incompetent "NBD1" composite site for many gating cycles has become viewed as a structural component that sustains integrity of the site throughout the multiple interface openings at the active site needed to allow ATP–ADP exchange each cycle (Aleksandrov et al., 2002; Basso et al., 2003; Tsai et al., 2010); and this view, of the dead site mostly remaining closed, has been incorporated into cartoons of the CFTR gating cycle (Gadsby et al., 2006; Csanády et al., 2010). Functional consequences of mutations within the NBD1–NBD2 interface have indeed indicated that NBD1 head–NBD2 tail contact across the catalytically dead site might be maintained (Tsai et al., 2010; Szollosi et al., 2011), although recent findings suggested relative NBD1–NBD2 motion in that dead site (Csanády et al., 2013).

Here, we directly address when, and how far, the NBD1–NBD2 heterodimer interface separates in each composite site during gating in functioning CFTR channels, by monitoring accessibility of introduced target cysteines (Karlin and Akabas, 1998). Before any NBD structure or evidence for NBD dimerization had been obtained, Cotten and Welsh (1998) probed ATP interactions with CFTR's NBDs by examining consequences of covalent modification by *N*-ethylmaleimide (NEM) of cysteines engineered into their Walker A and ABC signature motifs. They found ATP-induced opening of CFTR channels to be irreversibly impaired by NEM modification of each target cysteine (Cotten and Welsh, 1998). In the present work, we exploit reversible cysteine modification by MTS reagents to determine the gating-state dependence of accessibility of cysteines in CFTR's NBD1 and NBD2 signature sequences. By applying MTS reagents of varied size and charge to closed CFTR channels, or while the channels were freely opening and closing in the presence of ATP, we directly assessed the timing and extent of NBD1 and NBD2 separation during the gating and catalytic cycle. We find that cysteines in the signature sequences of both catalytic and noncatalytic sites are accessible when CFTR channels are closed, but not when the channels are open. The modification rates allow us to conclude that the NBD1–NBD2 interface separates by at least 8 Å at both composite sites every time a CFTR channel closes from an open burst.

MATERIALS AND METHODS

Molecular biology

The full-length human pGEMHE-CFTR (C832S-C1458S) construct, in which all eight C-terminal cysteines (C832, C866, C1344, C1355, C1395, C1400, C1410, and C1458 out of CFTR's 18 native cysteines) were replaced by serine, was generated by de novo PCR gene synthesis combined with site-directed mutagenesis (Mense et al., 2006). This template served for subsequent individual Ser-to-Cys mutations at positions 549, 605, and 1,347; Ala-to-Cys at 1,374 (Fig. S1); and the hydrolysis-impairing mutation K1250R, all introduced using QuikChange (Agilent Technologies). Point mutations in the pGEMHE–wild-type template (Chan et al., 2000) yielded C832S and S549C-C832S constructs (Figs. S2 B and S3). Mutations were confirmed by automated sequencing. cRNA was obtained by in vitro transcription.

Isolation and injection of *Xenopus laevis* oocytes

Xenopus oocytes were isolated as described previously (Chan et al., 2000), enzymatically defolliculated by mechanical agitation for 60–120 min in Ca^{2+}-free oocyte solution (mM: 82.5 NaCl, 2 KCl, 1 $MgCl_2$, and 5 HEPES, pH 7.5 with NaOH), supplemented with 0.2 Wünsch units/ml of Liberase Blendzyme 3 or Liberase TM Research Grade collagenase (Roche), and then given three 5-min rinses in Ca^{2+}-free solution to stop digestion before incubation at 18°C in the same solution supplemented with 1.8 mM $CaCl_2$ and 50 mg/ml gentamycin. The next day, selected oocytes (stage V–VI) were injected with 10–70 ng cRNA in 50 nl DEPC water and incubated for 3–6 d before recording.

Inside-out excised-patch current recording

After removal of vitelline membranes with forceps in standard bath solution (mM: 136 NMDG-Cl, 2 $MgCl_2$, 5 HEPES, and 0.5 EGTA, pH 7.2 with HCl), oocytes were transferred to a recording chamber on the stage of an inverted microscope (Nikon). Inside-out membrane patches were excised using 2–7-MΩ fire-polished pipettes (N-51-A capillaries; Drummond Scientific Company) filled with standard pipette solution (mM: 136 NMDG-Cl, 2 $MgCl_2$, and 5 HEPES, pH 7.4). Macroscopic holding current was recorded at a holding potential of ±30 mV (CFTR channel-open probability is essentially voltage independent over this range; Cai et al., 2003) using an Axopatch 200A amplifier (Molecular Devices), digitized at 1 kHz with a Digidata 1322A (Molecular Devices), and stored on a PC hard drive using Clampex 9.0.2.05 (Molecular Devices). The reference Ag-AgCl pellet (World Precision Instruments, Inc.) in a 3-M KCl-filled well was connected to the recording chamber via a 5% agar/bath solution bridge. Patches were continuously superfused with flowing solutions, at 22–24°C, driven by gravity and selected with computer-controlled electric valves (General Valve Corporation). For every patch, transient maximal activation (Kuruma and Hartzell, 2000) of endogenous Ca^{2+}-dependent Cl^- channels by briefly exposing patches to bath solution containing 500 µM Ca^{2+} was used to confirm inside-out patch configuration, and to assess solution exchange speed from exponential fits to current decay time courses on Ca^{2+} withdrawal; for the patches that yielded data presented here, the time constant averaged 0.3 ± 0.02 s (n = 18) using a custom flow chamber, and 0.2 ± 0.02 s (n = 19) using a piezo-electric solution switcher (Burleigh LSS-3200; AutoMate Scientific, Inc.).

CFTR channels were activated by exposures to solution containing 150 or 300 nM PKA catalytic subunit (from 23 µM stock in 100 µM DTT; bovine cardiac PKA; Sigma-Aldrich) plus 3 mM MgATP (from 400 mM stock in NMDG-Cl; Sigma-Aldrich). The prephosphorylated channels were subsequently opened and closed by application and removal of 3 mM MgATP without PKA. 10 or 20 mM DTT (Sigma-Aldrich), made daily, was dissolved directly in the 136-mM NMDG-Cl bath solution. MTS reagents (Toronto Research Chemicals) and avidin (Thermo Fisher Scientific) were added to superfusing solutions shortly before use from 100-mM stock solutions (kept on ice), aqueous for 2-trimethylammonium-ethyl-MTS ($MTSET^+$), 2-sulfonato-ethyl-MTS ($MTSES^-$), and 2-aminocarbonyl-ethyl-MTS (MTSACE), and in DMSO for MTS-rhodamine (2-sulfo-rhodamine-ethyl-MTS), MTS-glucose ((β-D-glucopyranosyl)-*N*-urea-*N'*-2-ethyl-MTS), and MTS-biotin (*N*-biotinylamino-ethyl-MTS); avidin stock solution was 300 µM in NMDG-Cl. Stocks were frozen at −20°C, and aliquots were thawed for experiments.

Current decay time courses upon washout of ATP, exposure to MTS reagent in the presence of ATP, or washout of both MTS reagent and ATP were fitted by single exponentials (Clampfit 10.3.1.4; Molecular Devices). For analysis, every time course was compared with that obtained for ATP withdrawal from the same channels, in the same patch, to account for variability in patch geometry inside the pipette tip, likely related to variations in tip size, expressed channel density, and membrane properties after collagenase digestion. Records and graphs in figures are plotted using OriginPro 7.0383 (OriginLab Corporation); all currents are displayed as outward (positive) for convenience. Results of analyses are presented as mean ± SEM of n measurements.

Structural models

Structures of TM287/288 (Protein Data Bank [PDB] accession no. 3QF4), Sav1866 (PBD accession no. 2ONJ), and the biotin–avidin complex (PDB accession no. 1AVD) were obtained from the Protein Data Bank; models of MTS reagents, NEM, and ATP were obtained from PubChem as lower energy conformers; and the structure of AMPPNP is from the TM287/288 crystal (PBD accession no. 3QF4). All structures were visualized using PyMOL (Molecular Graphics System; Schrödinger, LLC). The MTS-ethyl-amino moiety of MTS-biotin was manually appended to each biotin molecule in the biotin–avidin complex structure using the fragment builder in PyMOL. The sizes of MTS reagents, NEM, nucleotides, and biotin–avidin complex were assessed using Jmol 13.0.14 (http://www.jmol.org/) to calculate minimum bounding box dimensions needed to fit each molecule (for rotamers in Fig. 2), and these atom–center to atom–center distances were then increased by Van der Waals radii; the values were checked by direct measurement of space-filling structures in PyMOL.

Online supplemental material

Fig. S1 is a sequence alignment identifying the positions in TM287/288 and Sav1866 equivalent to the CFTR target positions studied here. Fig. S2 shows tests of $MTSET^+$, MTSACE, and $MTSES^-$ effects on ATP-activated currents of background (C832S-C1458S) or C832S CFTR channels lacking any target cysteine. Fig. S3 shows the action of $MTSET^+$ on the S549C target in the C832S background (missing only a single native cysteine) for comparison with the (C832S-C1458S) background. Fig. S4 summarizes data demonstrating that rates of current decay on MTS modification match those on ATP withdrawal regardless of >10-fold variation of absolute rates. Fig. S5 shows that MTS-glucose, MTS-rhodamine, and MTS-biotin do not affect background (C832S-C1458S) CFTR channels. Fig. S6 confirms that MTS-biotin retains activity when complexed with avidin by demonstrating that it modifies wild-type CFTR channels. The online supplemental material is available at http://www.jgp.org/cgi/content/full/jgp.201411347/DC1.

RESULTS

Targeting S549C in the NBD1 tail, in the catalytically competent site, of CFTR channels opening and closing in ATP

S549 in the LSGGQ sequence of the NBD1 tail contributes to CFTR's catalytically competent composite site

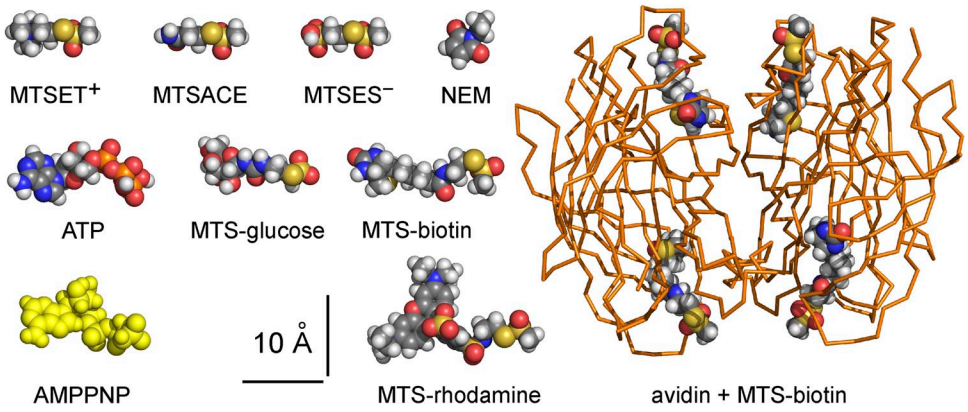

Figure 2. Size comparison of MTS reagents, nucleotides, NEM, and MTS-biotin–avidin complex, shown as CPK-colored spheres, except for AMPPNP (yellow spheres; from TM287/288 structure; PDB accession no. 3QF4) and avidin tetramer (orange ribbon). $MTSET^+$, MTSACE, and $MTSES^-$ all approximate cylinders ∼12 × ∼6-Å diameter, and NEM is ∼8 × ∼6-Å diameter. Minimum box sizes to fit low energy rotamers are shown: MTS-glucose, ∼16 × ∼8 × ∼7 Å; MTS-biotin, ∼19 × ∼7 × ∼6 Å; MTS-rhodamine, ∼22 × ∼14 × ∼8 Å; ATP, ∼19 × ∼9 × ∼8 Å; AMP-PNP, ∼19 × ∼9 × ∼6 Å; tetrameric avidin–MTS-biotin complex (PDB accession no. 1AVD) is ∼45-Å wide × ∼58-Å long.

and, by homology with nucleotide-bound NBD homodimer crystal structures, is expected to hydrogen bond to the γ phosphate of the ATP held by the NBD2 Walker A motif (Hopfner et al., 2000; Smith et al., 2002; Chen et al., 2003). To assess accessibility of introduced S549C, we applied the small hydrophilic, sulfhydryl-specific MTS reagent $MTSET^+$ (50 µM; Fig. 3 A) to S549C-(C832S-C1458S) CFTR channels opening and closing in inside-out patches exposed to 3 mM MgATP (Fig. 3 A). Despite the maintained presence of ATP, the $MTSET^+$ caused a rapid current decline (Fig. 3 A). The current decay reflects modification of the introduced cysteine because background (C832S-C1458S) CFTR channels, lacking the engineered target cysteine, are little affected (Fig. S2 A) by much higher concentrations of $MTSET^+$ or of the similarly sized MTS reagents, negatively charged $MTSES^-$, or neutral MTSACE; in these control (C832S-C1458S) CFTR channels, all eight native cysteines in the C-terminal half of CFTR have been replaced by serines, but all 10 native N-terminal cysteines remain (compare Mense et al., 2006). Near abolition of CFTR current by $MTSET^+$ while ATP was present indicates that CFTR channels with a covalently attached $MTSET^+$ adduct at position 549 can essentially no longer be opened by ATP. This corroborates impaired activity of S549C CFTR after permanent attachment of similarly sized (Fig. 2), but neutral, NEM (Cotten and Welsh, 1998).

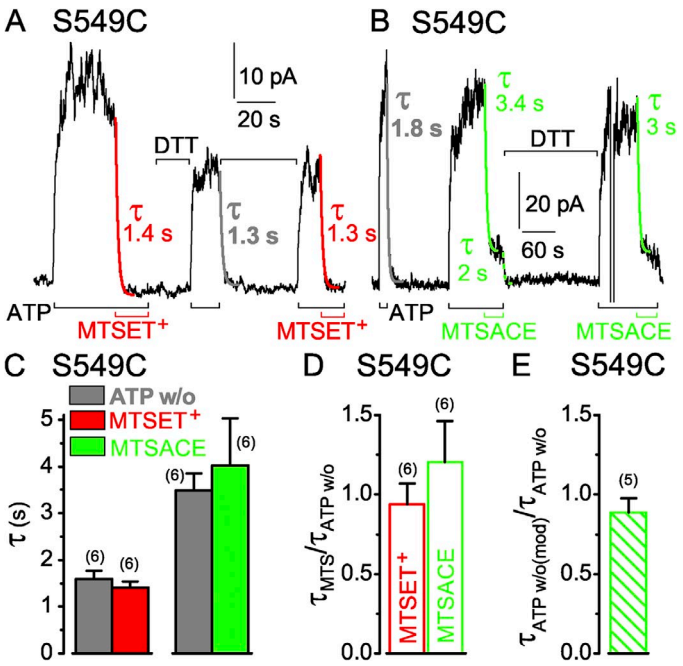

Figure 3. Similarly rapid decay of current in S549C CFTR channels (containing a single target Cys in the active catalytic site) upon ATP washout (w/o) or modification by MTS reagents. (A and B) S549C CFTR channels were activated by 3 mM ATP (black bars below records) and modified by 50 µM $MTSET^+$ (A; red bars below record) or 5 and 50 µM MTSACE (B; green bars below record), and modification was reversed by DTT (A, 10 mM; B, 20 mM; black bars above record). Colored lines show single-exponential fits to current decay time courses on modification (τ_{MTS}) by $MTSET^+$ (red) or by MTSACE (green), or on ATP removal (gray, $\tau_{ATPw/o}$) before modification, or on ATP removal after MTSACE modification (dotted green, $\tau_{ATPw/o(mod)}$); colored numbers give fit time constants; the time constants of Ca^{2+}-dependent Cl^- current decays in these patches were 0.3 s (A) and 0.2 s (B). (C) Average $\tau_{ATPw/o}$ with corresponding average τ_{MTS} from the same patches (left: gray bar, w/o, 1.6 ± 0.2 s; red bar, ≥50 µM $MTSET^+$, 1.4 ± 0.1 s; $n = 6$ measurements in five patches; right: gray bar, w/o, 3.5 ± 0.4 s; green bar, ≥50 µM MTSACE, 4.0 ± 1 s; $n = 6$ measurements in four patches); slower washout and modification time courses in the MTSACE experiments likely reflected slower superfusion influenced by patch geometry, but comparisons were always made within the same patch. (D) Averages of individual ratios of washout and modification time constants determined for each pair of measurements (from experiments of C; red open bar, $\tau_{MTSET}/\tau_{ATPw/o}$, 0.9 ± 0.1; green open bar, $\tau_{MTSACE}/\tau_{ATPw/o}$, 1.2 ± 0.3). (E) Average of washout time constant ratios, before and after MTSACE modification (green hatched bar, $\tau_{ATPw/o(mod)}/\tau_{ATPw/o}$, 0.9 ± 0.1; $n = 5$); absolute current amplitude of MTSACE-modified channels was 7–22 pA. Error bars represent mean ± SEM.

Exposure to the reducing agent DTT (10 mM) for ~20 s in the absence of ATP restored the ability of ATP to activate the channels; this demonstrates that DTT removed the $MTSET^+$ adduct, confirming that it was attached via a mixed disulfide bridge. The somewhat smaller size of the reactivated current could partly reflect incomplete adduct removal during the brief exposure to DTT. However, after further DTT treatment, ATP again activated a similar current, suggesting that partial dephosphorylation contributed to current diminution from the initial level (PKA catalytic subunit had been withdrawn 4 min before the start of this record). Reapplication of 50 µM $MTSET^+$ in 3 mM ATP once again rapidly decreased the current (Fig. 3 A).

Single-exponential fits (Fig. 3 A, red fit lines) yielded time constants of 1.4 and 1.3 s for $MTSET^+$-induced current decay in the presence of ATP in this recording. These values are closely similar to that, 1.3 s, for the intervening current decline caused by channel closure on abrupt ATP withdrawal (Fig. 3 A, gray fit line). If the ATP concentration at the cytoplasmic surface of the patch fell instantly to zero (the time constant of Ca^{2+}-activated Cl^- current decay on Ca^{2+} removal from this patch was 0.3 s), this time constant of current decline would report the mean open burst duration of the population of channels in the patch (Csanády et al., 2000, 2010). In each patch, the time courses of current decay on modification by a high concentration (≥50 µM) of $MTSET^+$ (Fig. 3 C, red bar) and on ATP withdrawal (Fig. 3 C, left gray bar) were comparable, as indicated by the near unity mean ratio of those time constants, 0.9 ± 0.1 (n = 6; Fig. 3 D, red open bar), obtained by averaging the time constant ratios found in each patch.

To confirm that this rapid $MTSET^+$ modification of S549C CFTR channels did not depend on the eight C-terminal cysteine-to-serine mutations, we tested modification of S549C CFTR that otherwise differed from wild-type by only the single mutation C832S needed to render CFTR unresponsive to NEM (Cotten and Welsh, 1997). The current decline on modification of S549C-C832S CFTR by $MTSET^+$ in 3 mM ATP (Fig. S3, red fit lines) was as rapid as that of S549C-(C832S-C1458S) CFTR (Fig. 3, A and C), and it similarly matched the time course of current decay on ATP washout (Fig. S3, gray fit line). However, because (C832S) background CFTR channels were slowly modified by $MTSES^-$ and MTSACE (Fig. S2 B), unlike (C832S-C1458S) background CFTR channels, which were insensitive to these reagents (Fig. S2 A), (C832S-C1458S) channels were adopted as the background for cysteine targets for the rest of this work.

We next tested whether impairment of channel opening by the $MTSET^+$ adduct simply reflected steric hindrance, independent of charge, by modifying S549C CFTR with neutral MTSACE (Fig. 3 B). The time constant of current decline on ATP withdrawal in the patch illustrated was 1.8 s (Fig. 3 B, gray fit line), and that of current decay on modification by a low concentration (5 µM) of MTSACE in the presence of ATP was somewhat slower, 3.4 s (Fig. 3 B, left green fit line). After adduct release by DTT, ATP activated almost the entire initial current, which was rapidly diminished by a 10-fold higher concentration (50 µM) of MTSACE (Fig. 3 B, right green fit line). The ratios of the time constants of current decline caused by ≥50 µM MTSACE (Fig. 3 C, green bar) and by ATP washout (Fig. 3 C, right gray bar) determined in each patch and averaged were again near unity (1.2 ± 0.3; n = 6; Fig. 3 D, green open bar).

Because modification by the MTS reagents is covalent, and their application in every experiment lasted for many (>5) reaction time constants, the reactions must have proceeded to completion. However, whereas that complete modification of a population of S549C channels by $MTSET^+$ almost abolished channel current, steady-state modification of the same channels by MTSACE instead diminished ATP-activated current by only ~80% (see Fig. 4 B). The residual current depended on the presence of ATP and must have arisen from modified S549C CFTR channels containing an MTSACE adduct, rather than from a subpopulation of channels that avoided modification. The latter explanation would require a different subpopulation of the same channels to evade modification by each reagent, to account for the different amplitude residual currents, and this seems unlikely. The residual current decayed rapidly upon ATP removal (e.g., Fig. 3 B, dashed green fit line), with a time constant similar to that for decline of current through the same channels when ATP was withdrawn before MTSACE modification (Fig. 3 B, gray fit line), as revealed by their near unity ratio (Fig. 3 E, green hatched bar). If the residual current does flow through MTSACE-modified S549C CFTR channels, this implies that the timing of channel closure was little influenced by the modification (see Implications of functional observations on modified channels in Discussion).

Modification of S549C in channels closed by removal of ATP

To see whether S549C CFTR channels can be modified when they are closed, the MTS reagents were applied after removing ATP. First, ATP was added to gauge channel activity, then ATP was withdrawn and 5 µM $MTSET^+$ was applied while the channels were closed (Fig. 4 A, red segment of current trace). After 60 s, $MTSET^+$ was removed and, simultaneously, the extent of modification assessed by reapplication of ATP, which in this instance activated little or no current. DTT was then applied to release the adduct, which restored activation of the control current amplitude by ATP. On average, exposure to 5 µM $MTSET^+$ for 60 s in the absence of ATP reduced the subsequent ATP-activated current to 6 ± 1% (n = 8) of the control amplitude (Fig. 4 B, left

red bar). This correlates well with the residual 4 ± 1% (n = 10) of control current after modification of S549C CFTR by ≥50 μM $MTSET^+$ applied in the presence of ATP (Fig. 4 B, right red bar; compare Fig. 3 A).

In the same patch, a 60-s exposure to 100 μM MTSACE without ATP (Fig. 4 A, green current trace) lowered the subsequent ATP-activated current on average to 18 ± 2% (n = 5) of the control amplitude (Fig. 4 B, left green bar). This residual current amplitude agrees well with that after ≥50 μM MTSACE modification of S549C CFTR with ATP present (18 ± 6%; n = 4; Fig. 4 B, right green bar; compare Fig. 3 B). Similarly, 100 μM $MTSES^-$ applied to the same patch for 60 s in the absence of ATP (Fig. 4 A, blue current trace) resulted in modified channels that yielded an ATP-activated current 17 ± 3% (n = 4) of the control amplitude (Fig. 4 B, blue bar).

Thus, closed S549C CFTR channels are readily modified by micromolar concentrations of $MTSET^+$, MTSACE, or $MTSES^-$. The diminished open probability of modified S549C channels in ATP is smaller when the covalently attached adduct has a positive charge ($MTSET^+$) than when it is neutral (MTSACE) or negatively charged ($MTSES^-$). Because unaltered decay rate of the residual current of MTSACE-modified S549C channels on ATP removal suggests little change in stability of the open state, this diminished open probability appears attributable (at least for the MTSACE adduct) to relative stabilization of the channel-closed state compared with unmodified S549C CFTR channels.

Targeting S1347C in LSHGH in the NBD2 tail, in the catalytically incompetent site, of CFTR channels opening and closing in ATP

The position equivalent to S549 in the signature motif of the noncatalytic composite site is S1347, in sequence LSHGH in the NBD2 tail. As with S549C channels, application of $MTSET^+$ (1 mM in the example in Fig. 5 A) to S1347C CFTR channels opening and closing in the presence of ATP caused rapid current decay, with a time constant (Fig. 5 C, red bar) comparable to that for current decline after ATP washout in the same patch (Fig. 5 C, left gray bar). The ratio of the time constants of current decay caused by ≥50 μM $MTSET^+$ and by ATP withdrawal averaged 1.0 ± 0.1 (n = 8; Fig. 5 D, red open bar). However, unlike the near abolition of S549C CFTR current caused by $MTSET^+$, modification of S1347C channels by $MTSET^+$ reduced ATP-activated current only by ∼60% (see Fig. 6 B). The residual current in $MTSET^+$-modified S1347C channels required ATP and declined on ATP withdrawal with a time course similar to that of the S1347C channels before modification (Fig. 5 E, red hatched bar). Thus, compared with unmodified S1347C channels, the presence of the $MTSET^+$ adduct appears to stabilize closed-channel states without greatly affecting the open burst duration.

S1347C CFTR channels opening and closing in ATP are also rapidly modified by MTSACE (1 mM in Fig. 5 B), causing current to decay with a time course closely similar to that seen on ATP washout (Fig. 5, B and C); the ratio of these time constants for ≥50 μM MTSACE averaged

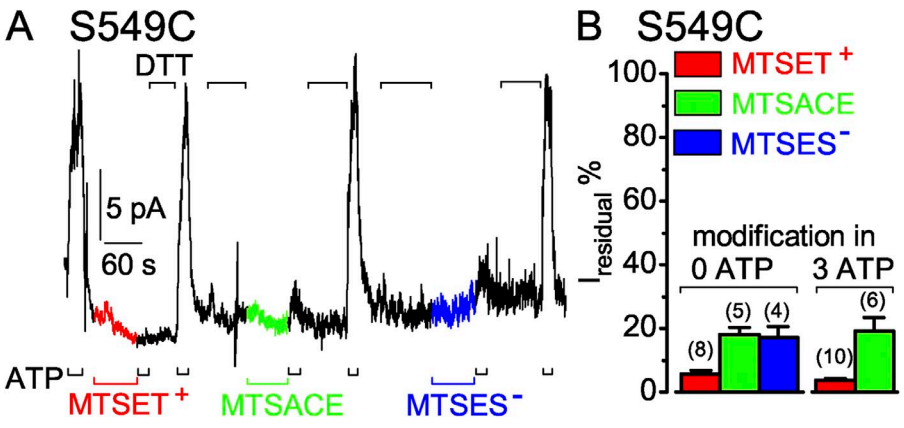

Figure 4. S549C CFTR channels are readily modified by MTS reagents when closed. (A) Immediately after 60-s applications of 5 μM $MTSET^+$ (red trace and bar), 100 μM MTSACE (green trace and bar), or 100 μM $MTSES^-$ (blue trace and bar) to closed S549C channels in the absence of ATP, brief exposures to 3 mM ATP (black bars below record) assessed residual channel activity; the time constant of Ca^{2+}-dependent Cl^- current decay in this patch was 0.2 s. Exposures to 10 mM DTT (black bars above record) fully restored ATP-activated current by releasing adducts after each modification. (B) Relative amplitude of residual ATP-dependent current ($I_{residual}$ %) of modified S549C channels. For modification while channels were closed (left, 0 ATP), residual ATP-activated current (peak current a few seconds after adding ATP minus baseline current just before ATP addition) of modified channels was compared with the average of peak ATP-activated currents of the same channels after full recovery from modification, and just before modification by $MTSET^+$ (red bar, 6 ± 1%; n = 8 measurements in six patches), by MTSACE (green bar, 18 ± 2%; n = 5 measurements in four patches), or by $MTSES^-$ (blue bar, 17 ± 3%; n = 4 measurements in three patches). For modification while channels were opening and closing in ATP (right, 3 mM ATP), residual ATP-dependent current (measured as the difference before and after ATP removal) of modified channels was compared with ATP-activated current of the same channels immediately before modification by ≥50 μM $MTSET^+$ (red bar, 4 ± 1%; n = 10 measurements in five patches) or by ≥50 μM MTSACE (green bar, 18 ± 6%; n = 4 measurements in four patches). Error bars represent mean ± SEM.

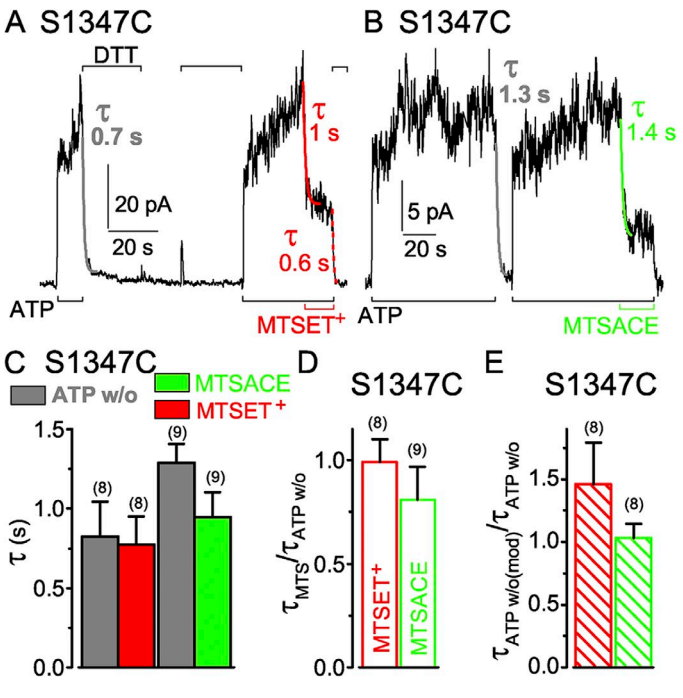

Figure 5. Similarly rapid decay of current in S1347C CFTR channels (containing a single target Cys in the dead composite site) upon ATP washout (w/o) or modification by MTS reagents. (A and B) S1347C CFTR channels were activated by 3 mM ATP (black bars below records) and modified by 1 mM $MTSET^+$ or MTSACE (A and B, red and green bars below records, respectively). Colored lines show single-exponential fits to current decay time courses on modification (τ_{MTS}) by $MTSET^+$ (red) or by MTSACE (green), or on ATP removal (gray, $\tau_{ATPw/o}$) before modification, or on ATP removal after $MTSET^+$ modification (dotted red, $\tau_{ATPw/o(mod)}$); colored numbers give time constants; the time constants of Ca^{2+}-dependent Cl^- current decays in these patches were 0.1 s (A) and 0.3 s (B). (C) Average $\tau_{ATPw/o}$ (gray bars) with corresponding average τ_{MTS} from the same patches (left: gray bar, w/o, 0.8 ± 0.2 s; red bar, ≥50 µM $MTSET^+$, 0.8 ± 0.2 s; n = 8 measurements in six patches; right: gray bar, w/o, 1.3 ± 0.1 s; green bar, ≥50 µM MTSACE, 0.9 ± 0.2 s; n = 9 measurements in seven patches). (D) Averages of individual ratios of washout and modification time constants determined for each pair of measurements (from experiments of C; red open bar, $\tau_{MTSET}/\tau_{ATPw/o}$, 1.0 ± 0.1; green open bar, $\tau_{MTSACE}/\tau_{ATPw/o}$, 0.8 ± 0.2). (E) Ratio of washout time constants before and after $MTSET^+$ and MTSACE modification ($\tau_{ATPw/o(mod)}/\tau_{ATPw/o}$: red hatched bar, $MTSET^+$, 1.5 ± 0.3, n = 8 measurements in six patches; green hatched bar, MTSACE, 1.0 ± 0.1; n = 8 measurements in seven patches); absolute current amplitudes were 5–64 pA for $MTSET^+$-modified channels and 6–80 pA for MTSACE-modified channels. Error bars represent mean ± SEM.

0.8 ± 0.2 (n = 8; Fig. 5 D, green open bar). The ∼20% residual current of S1347C channels modified by MTSACE in ATP (see Fig. 6 B) declined on ATP removal with a similar time constant to that of unmodified S1347C channels (Fig. 5 E, green hatched bar). The MTSACE adduct therefore also appears to stabilize closed conformations of modified, relative to those of unmodified, S1347C channels, but to little influence the mechanism that times channel closing.

Modification of S1347C in channels closed by removal of ATP

Closed S1347C channels in the absence of ATP, like closed S549C CFTR channels, were readily modified by MTS reagents. 60-s exposures to 50 µM $MTSET^+$, MTSACE, or $MTSES^-$, with intervening applications of DTT to release each adduct (Fig. 6 A), each diminished the amplitude of current subsequently activated by ATP (Fig. 6, A and B). Residual ATP-activated currents of

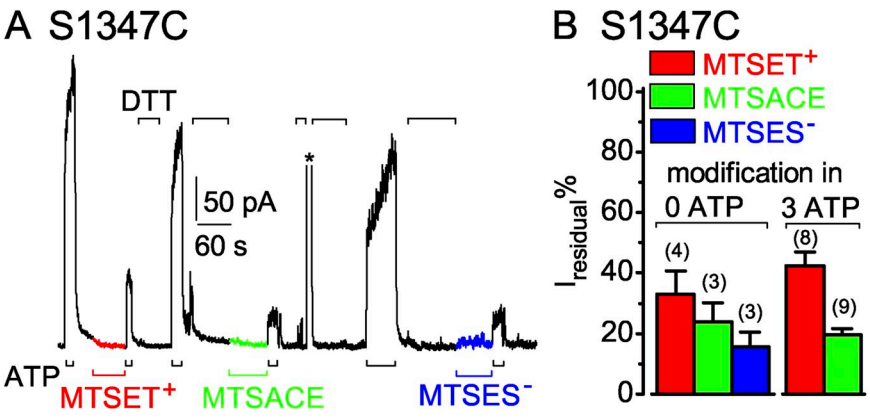

Figure 6. S1347C CFTR channels are readily modified by MTS reagents when closed. (A) Immediately after ∼60-s applications of 50 µM $MTSET^+$ (red trace and bar), MTSACE (green trace and bar), or $MTSES^-$ (blue trace and bar) to closed S1347C channels in the absence of ATP, brief exposures to 3 mM ATP (black bars below record) assessed residual channel activity. Exposures to 20 mM DTT (black bars above record) restored ATP-activated current by releasing adducts after each modification; the asterisk above the record marks brief activation of Ca^{2+}-dependent Cl^- current to monitor solution exchange speed (time constant = 0.3 s for this patch). (B) Amplitude of residual ATP-dependent current ($I_{residual}$ %), relative to ATP-activated current before modification, for S1347C channels modified, while closed (left, 0 ATP), by $MTSET^+$ (red bar, 33 ± 8%; n = 4 measurements in four patches), by MTSACE (green bar, 24 ± 6%; n = 3 measurements in three patches), or by $MTSES^-$ (blue bar, 16 ± 5%; n = 3 measurements in three patches), or while opening and closing (right, 3 mM ATP), by ≥50 µM $MTSET^+$ (red bar, 42.4 ± 4.5%, n = 8 measurements in four patches) or by ≥50 µM MTSACE (green bar, 19.5 ± 2.0%, n = 9 measurements in four patches). Error bars represent mean ± SEM.

S1347C CFTR channels after closed-state modification averaged 33 ± 8% (n = 4) after MTSET$^+$, 24 ± 6% (n = 3) after MTSACE, and 16 ± 5% (n = 3) after MTSES$^-$, of the control ATP-activated current amplitude before modification (Fig. 6 B, left; red, green, and blue bars). Those proportions were comparable to the average residual current amplitudes after modification of S1347C channels in the continued presence of ATP by MTSET$^+$, 42 ± 5% (n = 8), and by MTSACE, 20 ± 2% (n = 8) (Fig. 6 B, right; red and green bars).

Delaying closure of S549C and S1347C channels delays their modification

Evidently, engineered cysteines substituted for equivalent serines S549 in the catalytically active site and S1347 in the dead site are both readily accessible to small hydrophilic MTS reagents in closed CFTR channels. Also, the time course of current decay on modification of either cysteine by high concentrations of MTS reagents in the presence of ATP matches that of the current decay caused by channels shutting upon ATP withdrawal. A simple interpretation is that neither cysteine is accessible in open channels, so modification cannot occur until channels close, but is then so rapid that modification is complete before channels can reopen. If MTS reagents must indeed wait for channels to close to gain access to these interfacial NBD cysteines, then prolongation of the time each channel stays open would be expected to delay modification by the same factor.

Mutation of the conserved Walker A lysine to alanine or arginine in the active catalytic sites of P-gp (Lerner-Marmarosh et al., 1999) or CFTR (Ramjeesingh et al., 1999) abolishes ATP hydrolysis, and in CFTR, it substantially delays channel closure (Carson et al., 1995; Gunderson and Kopito, 1995). In CFTR channels mutated at NBD2 Walker A K1250, open burst durations are prolonged by about one (K1250R) or two (K1250A) orders of magnitude, in oocyte patches at room temperature (Vergani et al., 2003, 2005; Csanády et al., 2006). Accordingly, the current decay time constant on ATP withdrawal from S549C or S1347C CFTR channels bearing the K1250R mutation was slowed approximately 10-fold, to ∼15 s (Fig. 7, A–C, gray fit curves and bars). Moreover, modification of both target cysteines, S549C by 50 µM MTSET$^+$ (Fig. 7 A) and S1347C by 50 µM MTSACE (Fig. 7 B), was similarly slowed (Fig. 7, A–C). The ratios of the current decay time constants upon MTS modification in the presence of ATP (Fig. 7 C, red and green bars) to those upon ATP washout (Fig. 7 C, gray bars) therefore remained near unity, averaging 1.2 ± 0.2 (n = 3) for MTSET$^+$ action on S549C-K1250R, and 1.2 ± 0.1 (n = 7) for MTSACE action on S1347C-K1250R (Fig. 7 D, red and green open bars).

The matching time courses of current decline caused by ATP removal or to MTS modification of either target cysteine, S549C or S1347C, despite over an order of magnitude variation of the absolute values of both time constants (Figs. 3 D, 5 D, 7 D, and S4), strongly support strict state dependence of accessibility of the target cysteines. They suggest that modification of these interfacial cysteines by these small hydrophilic MTS reagents, and by inference reagent access, is restricted to closed-channel conformations after NBD separation. Target inaccessibility while channels are open is reasonably explained by the tight NBD1–NBD2 heterodimerization expected to follow ATP binding, by analogy with structural evidence from other ABC transporters (e.g., Smith et al., 2002; Chen et al., 2003; Dawson and Locher, 2006, 2007). Experimental functional evidence indeed strongly suggests that ATP-induced tight dimerization, at least at CFTR's catalytically active NBD2 composite

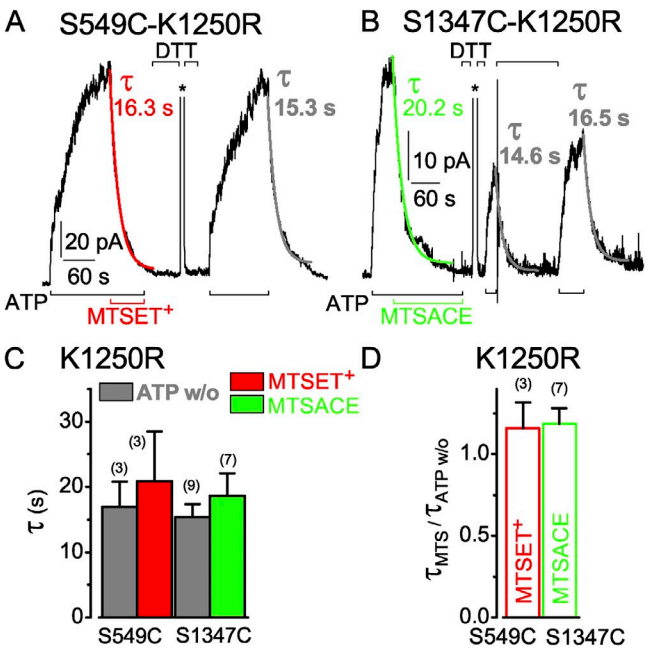

Figure 7. Hydrolysis-impairing mutation, K1250R, of the conserved Walker A lysine in the active composite site similarly slows current decay after ATP washout and upon MTS modification of both S549C and S1347C channels. (A and B) ATP-activated (3 mM, black bars below records) currents of S549C-K1250R (A) and S1347C-K1250R (B) CFTR channels with single-exponential fits to current decline upon ATP removal (gray, $\tau_{ATP\ w/o}$) or modification (τ_{MTS}) by 50 µM MTSET$^+$ (red) or MTSACE (green); 20 mM DTT (black bars above records) restored activation of currents by ATP; asterisks above the records mark brief activations of Ca^{2+}-dependent Cl^- currents to monitor speed of solution exchange (0.3 s in A and 0.2 s in B). (C) Average $\tau_{ATPw/o}$ (gray bars) with corresponding average τ_{MTS} from the same patches (left, S549C-K1250R: gray bar, w/o, 17 ± 3.8 s; red bar, MTSET$^+$, 20.9 ± 7.6 s; n = 3 measurements in three patches; right, S1347C-K1250R: gray bar, w/o, 15.4 ± 2.0 s; green bar, MTSACE, 18.6 ± 3.5 s; n = 9 and 7 measurements, respectively, in three patches). (D) Averages of individual ratios of washout and modification time constants determined for each pair of measurements (from experiments of C; red open bar, S549C-K1250R, $\tau_{MTSET}/\tau_{ATPw/o}$, 1.2 ± 0.2; green open bar, S1347C-K1250R, $\tau_{MTSACE}/\tau_{ATPw/o}$, 1.2 ± 0.1). Error bars represent mean ± SEM.

site (Vergani et al., 2005; Mense et al., 2006), causes opening of CFTR channels (Vergani et al., 2003; Csanády et al., 2006). The present results suggest that, as long as CFTR channels remain open, both target cysteines are buried and inaccessible in the dimer interface (compare Fig. 1, C and D). They further suggest that the ATP hydrolysis in the catalytically active site that normally prompts dimer disruption and ion channel closure causes sufficient separation of both active and inactive composite site interfaces to allow near instantaneous access of $MTSET^+$ and MTSACE to the conserved serine positions of both LSGGQ-like signature sequences.

Closed S549C channels are also readily modified by larger MTS reagents

The substituted ethyl-MTS reagents used so far, $MTSET^+$, MTSACE, and $MTSES^-$, all approximate cylinders ∼12 Å long and ∼6 Å in diameter (Fig. 2). For comparison with the various NBD separations observed in ABC exporter crystal structures, we tested whether larger MTS reagents could also access the NBD1–NBD2 interface in functioning CFTR. We first examined S549C CFTR channels closed by withdrawal of ATP, as in Figs. 4 and 6. Indeed, exposure to 20 µM MTS-glucose for ∼60 s diminished subsequent current activation by ATP (Fig. 8 A) to ∼7% of the control amplitude (Fig. 8 C), demonstrating that the ∼16 × ∼8 × ∼7–Å reagent (Fig. 2) could readily reach the target cysteine. The deposited adduct was partially removed by a 30-s application of DTT, and completely removed by further DTT treatment, as judged by restoration of ATP-activated current amplitude (Fig. 8 A). Larger still MTS-rhodamine (∼22 × ∼14 × ∼8 Å; Fig. 2), applied for 60 s at 5 µM (Fig. 8 A) also readily modified closed S549C CFTR (Fig. 8 A), diminishing ATP-activated current to ∼5% of control (Fig. 8 C). The MTS-rhodamine adduct appeared to be more slowly removed by DTT than the MTS-glucose adduct (Fig. 8 A).

The ∼19 × ∼7 × ∼6–Å (Fig. 2) reagent MTS-biotin (5 µM for 30 or 60 s; Fig. 8 B) similarly modified closed S549C CFTR channels, on average diminishing ATP-activated current to ∼15% of control (Fig. 8 C), and the modification was promptly reversed by DTT (Fig. 8 B). Control measurements with 50-µM applications of each of these larger MTS reagents confirmed that (like the smaller reagents; Fig. S2 A) they did not affect background (C832S-C1458S) CFTR channels with no added target cysteines (Fig. S5). The easy access of MTS-biotin, and its ready reversibility, allowed tests of accessibility of its tetrameric complex with avidin, expected to fit into any space ≥45-Å wide (Fig. 2). After a 60-s application of 5 µM MTS-biotin–avidin complex, however, ATP could still activate a large current, indicating that the cysteine at position 549 remained essentially unmodified (Fig. 8, B and C). Subsequent reexposure to MTS-biotin alone (without intervening DTT treatment) modified the cysteine, signaled by diminished ATP-activated current (Fig. 8 B); this confirmed that the cysteine had remained available and, hence, that the MTS-biotin–avidin complex had failed to act. That failure cannot be attributed to an inability of MTS-biotin to react with available cysteines while it is bound in the avidin tetramer, because 5 µM MTS-biotin–avidin complex readily modified, and stimulated, wild-type CFTR (Fig. S6), which contains 18 native cysteines; that covalent modification was reversed by DTT and could then be mimicked

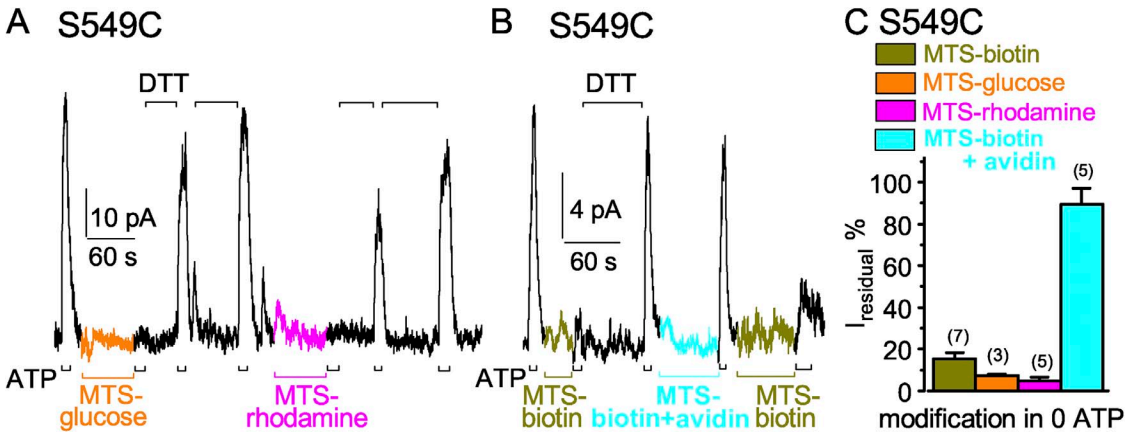

Figure 8. Larger MTS reagents also readily modify S549C CFTR channels when they are closed. (A and B) ATP-activated current (3 mM, black bars below record) was strongly diminished after modification of closed S549C CFTR channels by ≤60-s exposures to larger MTS reagents, 20 µM MTS-glucose (A; orange bar), 5 µM MTS-rhodamine (A; magenta bar), 5 µM MTS-biotin (B; dark yellow bar), and MTS-biotin–avidin complex (B; 5 µM biotin plus 5 µM avidin, cyan bar), all in the absence of ATP; 10 mM DTT (black bars above records) released adducts after each modification; the time constants of Ca^{2+}-dependent Cl^- current decays in these patches were 0.5 s (A) and 0.2 s (B). (C) Amplitude of residual ATP-activated current ($I_{residual}$ %), relative to ATP-activated current before modification, for S549C channels modified, while closed (in 0 ATP), by MTS-biotin (dark yellow bar, 15 ± 3%, n = 7 measurements), by MTS-glucose (orange bar, 7 ± 1%, n = 3 measurements), by MTS-rhodamine (magenta bar, 5 ± 2%, n = 5 measurements), or by MTS-biotin–avidin complex (cyan bar, 90 ± 8%, n = 5 measurements). Error bars represent mean ± SEM.

by 5 µM MTS-biotin alone (Fig. S6). Wild-type CFTR was previously shown to be irreversibly stimulated by NEM (Cotten and Welsh, 1997). We conclude, therefore, that the MTS-biotin–avidin complex failed to modify S549C in the catalytically competent site in closed CFTR channels because separation of the NBD1 tail from the NBD2 head was insufficient to allow the complex to reach the target cysteine. Thus, NBD1–NBD2 separation at the active site, when CFTR channels are closed after withdrawal of ATP, cannot be as large as 45 Å.

Larger MTS reagents also modify S1347C channels opening and closing in ATP

Target cysteine 1347, in the inactive composite site, was also readily modified by MTS-glucose, MTS-biotin, and MTS-rhodamine. To gauge the speed of modification, the reagents were applied to S1347C channels opening and closing in the presence of ATP (Fig. 9, A and B). All three larger MTS reagents diminished S1347C CFTR current relatively rapidly, to a residual level ~15% of the control ATP-activated current before modification (Fig. 9 C). Comparison, in the same patch, of the current decay time courses from modification and from ATP washout showed that, on average, the current decline caused by 50 µM MTS-biotin was 1.6-fold slower (n = 3), by 50 µM MTS-glucose was 2.4-fold slower (n = 3), and by 50 µM MTS-rhodamine was 3.4-fold slower (n = 3) than current decline on withdrawal of ATP (e.g., Fig. 9 B). Using, instead, time courses of modification by 50 µM MTSACE as reference (e.g., Fig. 9 A), modification by MTS-biotin was 1.3-fold slower (n = 1), by MTS-glucose was 2.1-fold slower (n = 2), and by MTS-rhodamine was threefold slower (n = 1).

When MTS-biotin–avidin complex was added to S1347C channels in the presence of ATP, or was added with ATP during channel activation (e.g., Fig. 9 B), the current was not diminished (Fig. 9, B and C). In either case, subsequent application of noncomplexed MTS-biotin or MTS-glucose (Fig. 9 B) without intervening DTT treatment caused rapid current decline, confirming that the MTS-biotin–avidin complex had left the target cysteine unmodified and, hence, available.

These findings demonstrate that, when CFTR channels close, the NBD1 head (in the inactive composite site) must separate promptly from the NBD2 tail by a distance that permits MTS reagents as large as MTS-rhodamine to modify the Cys at position 1347, but not far enough to allow access of the ~45-Å avidin tetramer containing MTS-biotin.

As noted for the smaller MTS reagents, the residual current of S1347C channels covalently modified with these larger adducts decayed rapidly once ATP was removed (e.g., Fig. 9, A and B); when they could be compared, the time courses matched (within a factor of 2) those observed before modification for MTS-biotin (n = 3), MTS-glucose (n = 3), and MTS-rhodamine (n = 2).

Modification of mid-interface target cysteines

To complement the tests of accessibility within the two composite nucleotide sites, we also examined interfacial target cysteines introduced midway between them, in place of NBD1 residue S605 (equivalent to H-loop

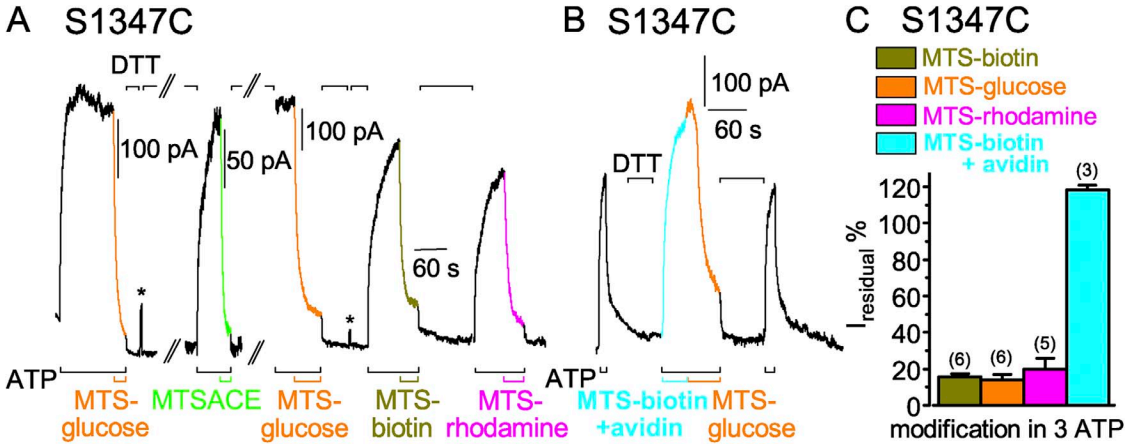

Figure 9. Larger MTS reagents relatively rapidly modify S1347C CFTR channels in the presence of ATP. (A and B) S1347C channels were activated by 3 mM ATP (black bars below records) and modified by 50 µM MTS-glucose (A and B; orange traces and bars), 50 µM MTSACE (A; green trace and bar), 50 µM MTS-biotin (A; dark yellow trace and bar), or 50 µM MTS-rhodamine (A; magenta trace and bar), but not by the MTS-biotin–avidin complex (B; 50 µM biotin plus 60 µM avidin, cyan trace and bar). Each modification was reversed by 20 mM DTT (A and B; black bars above record). Asterisks above the record in A mark brief activations of Ca^{2+}-dependent Cl^- currents to monitor speed of solution exchange (here, 0.3 s and 0.2 s); the gaps in A omit 30 and 450 s, and during the second gap the channels were rephosphorylated with PKA catalytic subunit. (C) Amplitude of residual ATP-activated current ($I_{residual}$ %), as a fraction of ATP-dependent current before MTS treatment, for S1347C channels modified, while opening and closing (in 3 mM ATP), by MTS-biotin (dark yellow bar, 16 ± 2%, n = 6 measurements in six patches), by MTS-glucose (orange bar, 14 ± 3%, n = 6 measurements in three patches), by MTS-rhodamine (magenta bar, 18 ± 6%, n = 6 measurements in five patches), and MTS-biotin–avidin complex (cyan bar, 119 ± 2%, n = 3 measurements in two patches). Error bars represent mean ± SEM.

consensus histidine; Fig. S1) or of NBD2 residue A1374 (equivalent to D-loop consensus serine). A cysteine pair at these positions can be cross-linked in functioning split CFTR channels in vivo— across the dimer interface—by membrane-permeant bismaleimidoethane, a bifunctional reagent with sulfhydryl-specific reactive groups ~8 Å apart (Mense et al., 2006).

The current of S605C CFTR channels opening and closing in the presence of ATP declined rapidly on modification by 1 mM $MTSET^+$ (Fig. 10 A). The time course was similar to that of the current decay when the channels were closed by ATP removal before modification (Fig. 10, A–C). The ~20% residual current of $MTSET^+$-modified S605C channels (Fig. 10 D) declined with a comparable time course to that of the unmodified channels on ATP withdrawal (Fig. 10, A and E). Unlike the readily reversible modification of S549C or S1347C targets, however, the $MTSET^+$ adduct was only poorly, if at all, released from $MTSET^+$-modified S605C channels by up to 85-s exposures to 10 mM DTT.

A1374C CFTR channels, with the target in the NBD2 D-loop, were also readily modified by $MTSET^+$ applied in the absence (Fig. 11 A) or presence of ATP (Fig. 11 B), in either case leaving a residual current 10–20% of control (Fig. 11 C). On average, the time course of current decay on modification with $MTSET^+$ was approximately twofold slower (mean of three measurements with 10 µM, and one with 1 mM, $MTSET^+$) than current decline on withdrawal of ATP (Fig. 11 D). In contrast to the irreversible modification of S605C channels, the $MTSET^+$ adduct could be released from modified A1374C channels by treatment with DTT (Fig. 11, A and B).

Thus, target cysteines introduced along the length of the NBD1–NBD2 heterodimer interface, from one composite site to the other, become promptly accessible to MTS reagents when CFTR channels close.

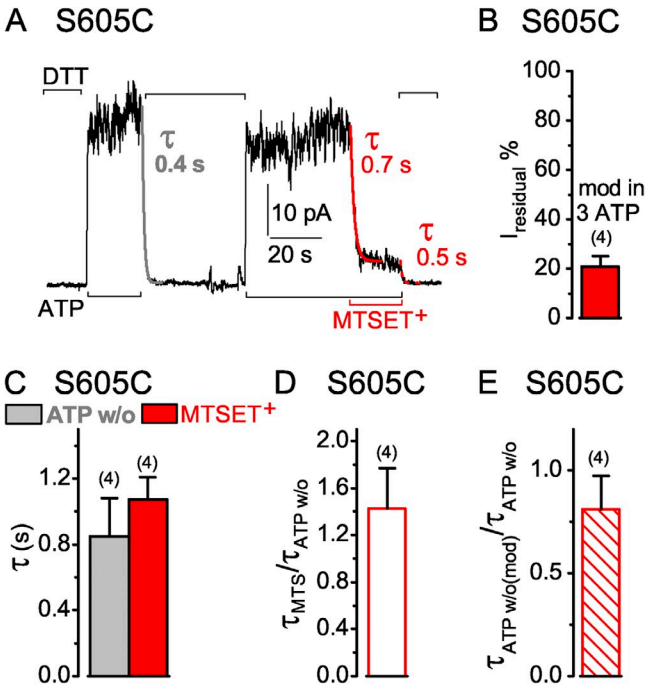

Figure 10. Similarly rapid decay of current in S605C CFTR channels (containing a mid-interface target Cys—in the NBD1 H loop—between the two composite sites) upon ATP washout (w/o) or modification by $MTSET^+$. (A) S605C-(C832S-C1458S) CFTR channels were activated by 3 mM ATP (black bars below records) and modified by 1 mM $MTSET^+$ (red bar). 10 mM DTT (black bars above record) kept the thiol reactive but could not remove the $MTSET^+$ adduct. Colored lines show single-exponential fits to current decay time courses on modification by $MTSET^+$ (red, τ_{MTS}), or on ATP removal (gray, $\tau_{ATPw/o}$) before modification, or on ATP removal after $MTSET^+$ modification (dotted red, $\tau_{ATPw/o(mod)}$); colored numbers give time constants. (B) Amplitude of residual current ($I_{residual}$ %), relative to ATP-activated current before modification, for S605C channels modified in 3 mM ATP by 1 mM $MTSET^+$ (red bar, 21 ± 4%, $n = 4$ measurements in four patches). (C) Average $\tau_{ATPw/o}$ (gray bar, w/o, 0.9 ± 0.2 s; $n = 4$ measurements in four patches) with corresponding average τ_{MTS} (red bar, $MTSET^+$, 1.1 ± 0.1 s) from the same patches. (D) Average of individual ratios of washout and modification time constants determined for each pair of measurements (from experiments of C; red open bar, $\tau_{MTSET}/\tau_{ATPw/o}$, 1.5 ± 0.3). (E) Ratio of washout time constants before and after $MTSET^+$ modification ($\tau_{ATPw/o(mod)}/\tau_{ATPw/o}$: red hatched bar, 0.9 ± 0.2, $n = 4$ measurements in four patches); absolute current amplitudes were 13–32 pA for $MTSET^+$-modified channels. Error bars represent mean ± SEM.

DISCUSSION

We monitored effects on CFTR channel activity of chemical modification of cysteine targets introduced into CFTR's NBD1–NBD2 heterodimer interface as a measure of accessibility of each cysteine, to learn how often relative to the channel gating cycle, and how far apart, the dimerized NBDs separate at the two interfacial composite catalytic sites in functioning CFTR.

Timing, and gating-state dependence, of modification

Ready reversal of MTS modification of target cysteines S549C and S1347C by DTT reduction of the mixed disulfide bonds, to release the adducts deposited during the reaction with MTS reagents, allowed the CFTR channels in each patch to serve as their own controls. In particular, this facilitated direct demonstration that CFTR channels closed by removal of ATP could nevertheless by readily modified by MTS reagents. This closed-state modification, together with the parallel time courses of current decay during the reaction with higher concentrations of MTS reagents in the presence of ATP and during channel closure on ATP washout, even when the latter was slowed 10-fold by a hydrolysis-impairing mutation, indicates that the channels could not be modified when they were open, but that they were very rapidly modified as soon as they closed. Moreover, modification of the target cysteine was equally rapid for both composite sites. For both sites, the parallel current decays upon modification or upon ATP

removal argue that, once closed, each channel was modified before it could reopen. In other words, on average, every channel reacted with MTS reagent in a single gating cycle. This stoichiometric modification diminished the open probability of every channel, in some instances to almost zero, despite the maintained presence of millimolar ATP.

The inferred protection from modification of open channels can be ascribed to inability of the MTS reagents to access either interfacial cysteine target while a channel is open. This is not surprising given the evidence that CFTR's open-channel state corresponds to an outward-facing conformation of the transmembrane domains and to tightly dimerized NBDs that enclose an ATP in both interfacial composite sites (Gadsby et al., 2006; Chen and Hwang, 2008). Although no crystal structure of CFTR, or of CFTR's dimerized NBDs, is available yet, crystal structures of nucleotide-bound homodimeric ABC transporters (e.g., Sav1866; Fig. 1, C and D) confirm the absence of space for entry of an MTS reagent into either composite nucleotide site, as well as the inaccessibility of both LSGGQ serines because of their interaction with occluded nucleoside triphosphate. Evidence that S549 (NBD1 tail) does indeed closely approach Walker A residue S1248 (NBD2 head) across the dimer interface in open CFTR channels comes from the demonstration that a Cu^{2+}-phenanthroline–induced disulfide bond between cysteine pair S549C and S1248C keeps the channels in prolonged open burst states long after removal of ATP (Mense et al., 2006). In addition, mutant cycle analysis indicates that NBD2 Walker A T1246 hydrogen bonds to NBD1 R555, adjacent to LSGGQ, in CFTR channels opened by ATP but not in closed channels (Vergani et al., 2005); the equivalent residue pair is seen to form an inter-NBD hydrogen bond only in nucleotide-bound tight NBD dimers (e.g., Smith et al., 2002; Chen et al., 2003; Zaitseva et al., 2005) and appears to have been subject to coevolution to maintain the distance between their α carbon atoms (Vergani et al., 2005). The inaccessibility of S1347C in open CFTR channels suggested by the present results argues that in the open-channel conformation, NBD1 and NBD2 are closely apposed also in the dead composite site, as they are in the active site (see below, Implications of functional observations on modified channels).

The NBD1–NBD2 dimer interface at CFTR's active composite site must separate each catalytic cycle to allow fresh ATP to replace the hydrolysis products, ADP and Pi. Given the strict temporal coupling between gating and catalytic cycles—i.e., each open burst is terminated by hydrolysis of a single ATP (established for wild-type CFTR, as well as for CFTR with dead site mutations in either NBD1 head or NBD2 tail; Csanády et al., 2010, 2013)—this requirement for active site opening each gating cycle can therefore account for the observed pattern of active site accessibility to nucleotide-sized MTS reagents. However, we found equally rapid modification of the equivalent cysteine in the dead composite site, meaning that the signature-sequence cysteine in that site also must have become accessible to MTS reagents each gating, and catalytic, cycle. Moreover, relatively rapid modification, on the time scale of the gating cycle, of interfacial target cysteines S605C and

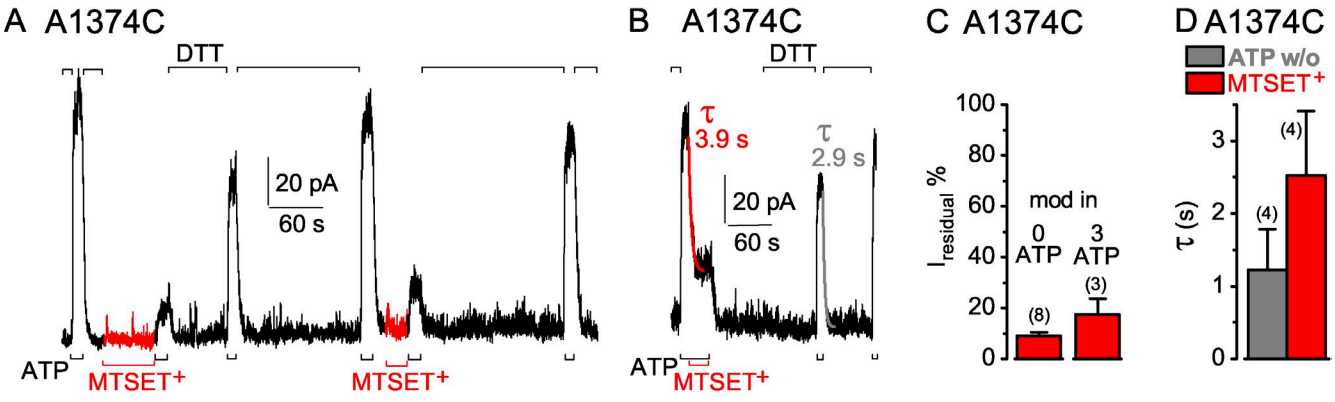

Figure 11. Rapid decay of current in A1374C CFTR channels (containing a mid-interface target Cys—in the NBD2 D loop—between the two composite sites) upon ATP washout (w/o) or modification by $MTSET^+$. (A and B) A1374C-(C832S-C1458S) CFTR channels were modified by 1 mM $MTSET^+$ (red trace bar) either while closed in the absence of ATP (A), as assessed by subsequent diminished ATP-activated current (3 mM, black bars below records), or in the presence of ATP (B). 10 mM DTT (black bars above record) removed the $MTSET^+$ adduct after each modification. (B) Colored lines show single-exponential fits to current decay time courses on modification by $MTSET^+$ (red, τ_{MTS}), or on ATP removal (gray, $\tau_{ATPw/o}$); colored numbers give time constants. (C) Amplitude of residual current ($I_{residual}$ %), relative to ATP-activated current before modification, for A1374C channels modified, while closed (left, 0 ATP), by 5 µM–1 mM $MTSET^+$ (red bar, 9 ± 2%; n = 8 measurements in six patches), or while opening and closing (right, 3 mM ATP), by 10 µM–1 mM $MTSET^+$ (red bar, 17 ± 6%, n = 3 measurements in two patches). (D) Average $\tau_{ATPw/o}$ (gray bar, w/o, 1.2 ± 0.6 s; n = 4 measurements in three patches) with corresponding average τ_{MTS} (red bar, $MTSET^+$, 2.5 ± 0.9 s) from the same patches. Error bars represent mean ± SEM.

A1374C, located between the two composite sites, implies separation all along the dimer interface each cycle.

Reaction rates are high

Consideration of the rate of MTS reagent reaction with each cysteine provides a gauge of how accessible they are. In a single patch of S549C channels subjected to repeated exposures to three concentrations of $MTSET^+$ in ATP, the mean current decay time constant in response to near saturating, 1 mM, $MTSET^+$ was 1.1 ± 0.1 s (n = 4), to 50 µM $MTSET^+$ was 1.9 ± 0.1 s (n = 8), and to 5 µM $MTSET^+$ was 4.0 ± 0.2 s (n = 6), whereas a further approximately ninefold slowing was observed in other patches on lowering [$MTSET^+$] from 5 to 0.5 µM. These lower modification rates at low micromolar [$MTSET^+$] were evidently limited by reagent concentration. But at the highest concentrations, the apparently asymptotic reaction rate became limited by a step approximately fivefold slower than solution exchange (time constant 0.2 s for this patch), supporting the conclusion that modification is rate limited by channel closure.

From the approximately linear dependence of reaction rate on reagent concentration at low micromolar levels, and the 4-s modification time constant at 5 µM, the second-order reaction rate constant for $MTSET^+$ modification of S549C is estimated to be $5 \times 10^4\ M^{-1}s^{-1}$. Because $MTSET^+$ access is limited to the fraction of time the channels spend closed, this value underestimates the true reaction rate constant by the factor 1-P_o (where P_o is channel-open probability). As P_o of Cys-free (16CS + C590V/C592V) CFTR was approximately twofold larger (Mense et al., 2006) than that of wild-type CFTR, which is ∼0.1 under these conditions (Csanády et al., 2000; Vergani et al., 2003), if P_o of these S549C-(C832S-C1458S) CFTR channels lies between these values, then our second-order rate constant estimate should be increased by up to 25%. Regardless of any correction, this lower estimate is only approximately fourfold smaller than the rate constant for $MTSET^+$ reaction with 2-mercaptoethanol in solution (Karlin and Akabas, 1998), at similar temperature, pH, and ionic strength as in the present experiments. This demonstrates that Cys549 is highly accessible in closed CFTR channels. Rapid accessibility did not depend on the positive charge of $MTSET^+$ because the second-order reaction rate constant for modification by the same sized but neutral MTSACE is similar (e.g., Fig. 3 B; 3.4-s decay time constant for 5 µM MTSACE).

Comparable analysis confirms that Cys1347 in the dead site was also rapidly accessible. The time constant of current decay during 11 modifications (in six patches) of Cys1347 by 5 µM MTSACE averaged 5.1 s, yielding an apparent second-order reaction rate constant of $4 \times 10^4\ M^{-1}s^{-1}$. As for Cys549, this underestimates true MTSACE reaction rate on Cys1347 because modification is precluded while channels are open. Also as for Cys549, reaction of Cys1347 with positively charged $MTSET^+$ is similarly rapid (Fig. 5, A–D).

Interpretation of accessibility in terms of NBD separation distance

These findings demonstrate that NBD dimerization keeps both signature sequences inaccessible in open CFTR channels, but that the NBDs separate sufficiently to make both signature motifs accessible every time a channel closes. Can we discern the extent of this NBD1 and NBD2 separation at each composite site? "Separation," as used throughout this paper, has an operational definition and refers to the minimal width of the access path from bulk (cytoplasmic side) solution to each target sulfhydryl; it does not preclude interaction between the NBDs elsewhere. The extended conformation adopted by ATP in solution, with or without bound Mg^{2+}, fits in a box ∼19 × ∼9 × ∼8 Å (e.g., Fig. 2). So, in each cycle, the NBD2 P-loop in the active site must separate far enough from the NBD1 signature sequence to open a space at least 8-Å wide for ADP to leave and ATP to enter and bind in its place at the NBD2 head. Therefore, if $MTSET^+$, MTSACE, and $MTSES^-$ approach targets in their ∼6-Å-wide extended conformations (Fig. 2), their ability to reach Cys549 of the NBD1 signature sequence is understandable. Similarly, MTS-glucose and MTS-biotin in extended conformations are comparable in size to ATP (Fig. 2), so their access is likewise explicable. But our assay is modification, not just access. This requires reaction between the reagent's MTS moiety and the cysteine thiolate to covalently attach the adduct to the cysteine sulfur via a mixed disulfide bond. The large rate constants estimated above for reaction of $MTSET^+$ and MTSACE with Cys549, approaching the free solution value for $MTSET^+$, imply that there is sufficient room for both the cysteine rotamer and the approach angles of the MTS reagents to rapidly assume favorable positions for productive reaction, and hence that they experience little spatial or geometric restriction.

The MTSACE reaction rate constant for modification of Cys1347 is also large, suggesting that the physical dimensions of the reaction cavity formed during each gating cycle by dimer separation at the dead site are comparable to those at the active site. The observed roughly twofold slowing of the modification rates of Cys1347 for MTS-biotin and MTS-glucose—and approximately threefold for MTS-rhodamine—compared with modification by $MTSET^+$ and MTSACE, suggests that even those larger reagents were able to enter the separated NBD interface and productively react with every channel within two, or three, gating cycles. A key distinction between the dead and active composite sites in CFTR, however, is that ATP is known to remain bound at the dead site, without being hydrolyzed, for many gating cycles (e.g., ∼50 cycles; Tsai et al., 2010). Analysis of tryptic digests (Aleksandrov et al., 2002, 2008) or of split

CFTR channels (Basso et al., 2003) showed that the nucleotide stays bound to the NBD1 head, not to the NBD2 tail (which includes position 1347). Intriguingly, in the structure of the heterodimeric ABC transporter TM287/288 (Fig. 1, A and B; Hohl et al., 2012) crystallized in the presence of AMPPNP, nucleotide is similarly found bound to the P-loop of TM287, equivalent to CFTR's NBD1 head; the other consensus, active catalytic site in TM287/288 is devoid of nucleotide, and the transmembrane domains are in an inward-facing conformation analogous to expectations for the closed-channel state of CFTR. It seems reasonable to assume that ATP remained tightly bound at the NBD1 head also in the present experiments, throughout the modification of Cys1347 by MTS reagents while channels were opening and closing in the presence of ATP. If so, that stably bound ATP must have narrowed the interfacial space accessible to MTS reagent by the width of the nucleotide. In other words, the NBD1–NBD2 separation in the dead site (e.g., NBD1 Walker A to NBD2 signature sequence) would have had to exceed that in the active site by a few angstroms to afford MTS reagents the same space in both sites in which to react with the signature sequence target cysteines. Whether or not ATP remained in the dead site, the similarly large reaction rates we observed for cysteines within the active and dead sites, on the order of rates for cysteines in free solution, suggest that in neither site was reaction limited by appreciable steric constraint.

Cotten and Welsh (1998), using the somewhat smaller (Fig. 2), neutral, lipohilic, and irreversible NEM, also reported rapid modification of cysteines in the same signature-sequence positions, at rates approaching those of thiols in solution. They studied S549C-C832S CFTR (compare Fig. S3) and S1347C-C832S CFTR channels, at 35°C, in patches excised from HeLa cells, and found modification of S1347C "slightly slower" than that of S549C, but nevertheless concluded that the signature sequence lies in a "solvent-exposed position" and "at the protein surface" (Cotten and Welsh, 1998). Their finding that those modification rates were little influenced by ATP concentration between 0.3 and 5 mM is now understandable. We now know that ATP binds only to closed CFTR channels, with separated NBDs (Vergani et al., 2005), and that in all ABC proteins, ATP first contacts the Walker motifs, because it is found there in all crystal structures of ATP-bound NBD monomers (e.g., Hung et al., 1998), including CFTR's NBD1 (e.g., Lewis et al., 2004); the bound ATP interacts with the signature sequence only after formation of the tight NBD1–NBD2 dimer. In a closed channel, therefore, with separated NBDs, accessibility of signature-sequence target cysteines to hydrophylic MTS reagents can now be expected to be independent of ATP concentration.

In contrast, Cotten and Welsh (1998) found that although a cysteine substituted for CFTR's NBD2 Walker A residue S1248, in the active site, was rapidly modified by NEM, diminishing current within seconds, a cysteine at the equivalent NBD1 Walker A position A462, in the dead site, was modified only very slowly by NEM, with current diminishing over minutes, even at 35°C. That modification at both sites slowed as [ATP] was raised (Cotten and Welsh, 1998) is now readily explained by bound ATP shielding both Walker target cysteines from NEM attack while NBDs are separated in closed CFTR channels. The disparate modification rates of the two Walker targets strongly support the current view of rapid nucleotide release from the NBD2 head at the active site but very slow release from the NBD1 head at the dead site (Aleksandrov et al., 2002; Basso et al., 2003; Vergani et al., 2003; Gadsby et al., 2006; Chen and Hwang, 2008; Tsai et al., 2010).

Cysteine substitution caveats

An important assumption underlying interpretation of these findings is that inferences about NBD motions derived from them apply equally well to wild-type CFTR as to the cysteine-depleted CFTRs with added cysteine target studied here. There are reasonable grounds for believing this is so. Considering cysteine removal first, even full-length cysteine-free CFTR channels, lacking all 18 native cysteines, function similarly to wild type (Cui et al., 2006; Mense et al., 2006; Bai et al., 2010), although with somewhat enhanced open probability (Mense et al., 2006; Bai et al., 2010) as a result of longer open burst durations (1.7 ± 0.3 s; $n = 18$) than wild type (0.4 ± 0.03 s; $n = 10$); importantly, their apparent ATP affinity for channel opening is unchanged (see Fig. S1 in Mense et al., 2006). The cysteine-depleted (C832S-C1458S) CFTR used as the background construct here lacks only eight native cysteines (via eight conservative Cys-Ser substitutions, from C832S to C1458S) and is the full-length (concatenated) version of the split CFTR (coexpressed halves) into which cysteine target pairs were introduced for cross-linking studies to define CFTR's NBD1–NBD2 interface (Mense et al., 2006). All those dual-target split CFTR constructs formed fully functional channels, just like the single-target full-length CFTR channels derived from them that were studied here. Further evidence that the isosteric replacement of eight native cysteines little affected the results is the fact that our findings with the S549C target mutation in NBD1 (Fig. 3 A) were reproduced in an almost native background CFTR (C832S) lacking only 1 of the 18 cysteines (Fig. S3); likewise, NEM was found to rapidly modify both S549C and S1347C targets introduced into that same C832S CFTR background (Cotten and Welsh, 1998).

Although alteration of NBD structure by introduction of the individual target cysteines cannot be ruled out without atomic-resolution structures of CFTR before and after mutation, several observations make it seem unlikely that our conclusions are influenced by substantial

structural distortion. Thus, three of the substitutions, including those in the signature sequences, involve conservative replacement of the oxygen atom of a serine side chain with a sulfur atom. The less conservative mutation S142A of the corresponding ABC signature serine, present in both LSGGQ sequences of homodimeric GlcV, the isolated NBDs of a prokaryotic glucose transporter, diminished their ATP hydrolysis rate by only ∼40% (Verdon et al., 2003). Even in CFTR channels, the nonconservative mutation S1347G in the NBD2 signature sequence diminished open burst duration, and open probability, by only about one third (Tsai et al., 2010). Consistent with these small effects, the mean time constant of current decay on ATP withdrawal, a measure of open burst duration, averaged 1.0 ± 0.1 s (n = 19) for our background (C832S-C1458S) CFTR channels (e.g., Fig. S2 A), and was unaltered after insertion of the dead-site signature-sequence target cysteine, S1347C (1.0 ± 0.1 s; n = 22), but was somewhat slowed by the corresponding cysteine in the live site, S549C (2.2 ± 0.2 s; n = 24). This suggests that hydrolysis of the ATP in the live site was mildly delayed by mutation of the signature-sequence serine that contacts its γ phosphate, but was unaffected by the equivalent Ser-Cys mutation in the dead site. That closure of (C832S-C1458S) channels containing S1347C or S549C target cysteines is indeed rate-limited by ATP hydrolysis (like wild type) is confirmed by the order of magnitude slowing of closure caused by the addition of the hydrolysis-impairing K1250R mutation (Figs. 7 and S4). Moreover, the ∼15-s time constants for nonhydrolytic closure of those S1347C-K1250R-(C832S-C1458S) and S549C-K1250R-(C832S-C1458S) channels upon ATP washout are no shorter than those, 6–9 s, of K1250R CFTR channels bearing no other mutation (Vergani et al., 2005; Csanády et al., 2006; Szollosi et al., 2010, 2011). All available evidence, therefore, indicates that channels containing the cysteine targets closed by the same mechanisms as those without; in particular, neither signature-sequence Ser-Cys mutation destabilized the prehydrolytic NBD1–NBD2 dimer, nor accelerated channel closure by ATP hydrolysis, arguing that the pattern of MTS reagent accessibility demonstrated here cannot be attributed to these conservative target mutations.

Given the lack of evidence for substantial distortion of the signature-sequence backbone by the Ser-to-Cys substitutions, possible differences between the positions of the Cys sulfur and the Ser oxygen caused by different side-chain rotamers ought to influence NBD separation estimates by only 1–2 Å, adequate for present purposes.

Interpretation of accessibility in terms of TM287/288 structure

How best to interpret CFTR NBD separation in terms of available ABC protein structures? As argued above, there are good reasons to believe MTS modifications of CFTR channels opening and closing in ATP occurred in closed channels with a nonhydrolyzed ATP bound to the NBD1 Walker motifs of the dead site and with the active site opened for ADP–ATP exchange. Absent a high resolution structure of CFTR, the structure of heterodimeric TM287/288 (Hohl et al., 2012), with a single AMPPNP bound to the TM287 P-loop in the degenerate site and with the catalytically active site vacant (Fig. 1, A–C), provides a reasonable starting point. The space-filling models show the hydroxyl oxygens of both signature-sequence serines (equivalent to CFTR's S549 and S1347) positioned ∼12 Å along the dimer interface from either end (Fig. 1 C), and ∼12 Å down from the upper (closer to the membrane) surfaces of the NBDs (Fig. 1, A and B). So, if CFTR's NBDs adopt a similar structure when the channels are closed, and the target sulfhydryls are in the positions of those oxygens, then all reactive MTS reagents used here must have penetrated the dimer interface to be able to react and form disulfide bonds. Indeed, the Fig. 1 (B and C) structures display interfacial clefts ∼10-Å wide that would allow access toward either target cysteine position over the roughly 90° arc going from horizontal (the line of vision in Fig. 1 B) to vertical (the line of vision in Fig. 1 C). The narrowest part of the pie-shaped segment of cleft within this 90° arc is at its apex, where in the dead site an ∼7-Å space would separate the target thiol from the tightly bound nucleotide (expected to be ATP in the present experiments), and in the active site ∼8 Å would separate the NBD1 tail thiol from the NBD2 head, vacant after departure of the hydrolysis product ADP (Fig. 1, B and C). The upper surfaces of the NBDs are also ≥10 Å apart in the midregion of the interface, forming a cavity between the composite sites (Fig. 1 C) and offering an alternative access route to the target thiols should MTS reagents enter between separated helical extensions of the transmembrane domains (Fig. 1, A and B). Together, these pathways would readily account for modification by $MTSET^+$, MTSACE, $MTSES^-$, MTS-biotin, and MTS-glucose, which in their approximately cylindrical extended conformations could all easily access the signature-sequence cysteine targets. MTS-rhodamine would also be expected to reach the cysteines, although with fewer degrees of freedom because of its T-shaped structure, so that its access would likely be somewhat restricted. That might account for the observed slightly slower modification of Cys1347 by MTS-rhodamine than by, e.g., MTSACE (Fig. 9 A). None of these pathways would permit access to either cysteine target of the 45-Å-wide MTS-biotin–avidin complex, also consistent with observation.

In the AMPPNP-bound TM287/288 structure, the residues at the mid-interface target positions equivalent to NBD1 S605 and NBD2 A1374 interact across the dimer interface through a hydrogen bond network that includes the tightly bound nucleotide's phosphates;

and although no impediment to accessibility of A1374 equivalent in the D-loop is evident (Fig. 1 C), the S605 (switch histidine) equivalent appears less open. However, cysteines introduced at either location in CFTR are rapidly modified by $MTSET^+$ (Figs. S6 and S7), and so both must be easily accessible; the reason for the impaired reversal of S605C modification by DTT is unclear but perhaps reflects electrostatic interaction with phosphates of the bound nucleotide.

A newer apo x-ray structure of TM287-288 (Hohl et al., 2014), devoid of any nucleotide, reveals little change in the position of the two NBDs. But, as expected, the lack of nucleotide at the NBD1 head of the dead site is observed to widen, by 2–5 Å, access pathways to the position equivalent to our Cys1347 target.

Comparison of patterns of accessibility with apo structures of ABC exporters

Several structures of inward-facing conformations of other ABC exporters crystallized in the absence of any nucleotide have been determined. Most show separation of the NBDs at least as wide as that seen in the TM287-288 structures and would thus, by that criterion alone, be compatible with the pattern of access we observed for MTS reagents targeting cysteines substituted for either signature-sequence serine, the serine in the NBD1 switch histidine position, or the alanine in the NBD2 D-loop serine position (Fig. S1). From space-filling models of these apo structures, we estimate the accessible cleft between separated NBDs at the depth of the signature sequence in each composite site to be ∼4-Å wide for VcMsbA (closed apo; PDB accession no. 3B5Y; Ward et al., 2007), ∼8 Å for ABCB10 (PDB accession no. 3ZDQ; Shintre et al., 2013), ∼13 Å for CmABCB1 (PDB accession no. 3WMG; Kodan et al., 2014), 15 and 14 Å for NaAtm1 (PDB accession no. 4MRN; Lee et al., 2014), 19 and 11 Å for MmP-gp (PDB accession no. 3G60; Aller et al., 2009), 20 and 19 Å for ScAtm1 (PDB accession no. 4MYC; Srinivasan et al., 2014), 34 and 28 Å for CeP-gp (PDB accession no. 4F4C; Jin et al., 2012), 35 and 31 Å for MmP-gp (PDB accession no. 4KSC; Ward et al., 2013), and 54 Å for EcMsbA (open apo; PDB accession no. 3B5W; Ward et al., 2007). It is unclear, however, whether any of these structures is appropriate for detailed interpretation of the accessibility of interfacial NBD targets in CFTR, because none is of an intrinsically asymmetric, heterodimeric ABC transporter like CFTR (and like TM287/288 and TmrAB). Moreover, in all these structures, both NBDs are devoid of nucleotide, whereas CFTR likely retained ATP in the dead site in the majority of the present experiments (like the equivalent site in TM287/288 contained AMPPNP; Hohl et al., 2012). In addition, whether such apo conformations occur during the catalytic cycle of any functioning ABC transporter has yet to be demonstrated.

An early model of the ABC transporter catalytic cycle proposed that ATP hydrolysis alternates between functionally equivalent catalytic sites (Senior et al., 1995), with products released from one site at a time (Tombline and Senior, 2005; Siarheyeva et al., 2010), because only a single post-hydrolytic vanadate-trapped ADP was found in each intact P-gp or $MalGHK_2$ transporter (e.g., Urbatsch et al., 1995; Fetsch and Davidson, 2002). A later "processive-clamp" model proposed that hydrolysis occurs at both sites before products are released together (Janas et al., 2003), because vanadate-trapped ADP was detected in both sites of isolated Mdl1P NBD homodimers (Janas et al., 2003) and of TmrAB transporters (Zutz et al., 2011). Unfortunately, methods with the kinetic resolution to learn whether hydrolysis products are released from one site at a time, or simultaneously from both sites, during a catalytic cycle have not yet been applied to any ABC transporter. Although the results presented here show that CFTR's NBDs separate sufficiently at both sites each catalytic cycle to allow access to both signature sequences, and ATP–ADP exchange at the live site, they do not directly address nucleotide exchange at the dead site; and, because only one site in CFTR is capable of hydrolysis, the implications of these results for ABC proteins that hydrolyze ATP in both sites remain uncertain.

We note again the failure in these experiments of 45-Å-wide tetrameric avidin, containing four MTS-biotin molecules (Fig. 2), to react with either signature-sequence target, Cys549 of NBD1 (Fig. 8) or Cys1347 of NBD2 (Fig. 9). This shows that functioning CFTR channels do not adopt any conformation with NBDs separated as widely as in the open apo MsbA structure (54 Å; Ward et al., 2007).

Comparison of accessibility patterns with ABC structures showing laterally offset NBDs

Evidence from some ABC exporters has suggested that NBD separation might not exclusively involve motion normal to the dimer interface. An additional lateral sliding motion along the dimer interface that moves the Walker A motifs toward each other and closer to the interface center (envision relative downward motion of blue TM288, in Fig. 1 C, and upward motion of green TM287, bringing the two red Walker A motifs together) has been posited as an essential driver of alternate conformations of the transmembrane helices (Ward et al., 2007; Moradi and Tajkhorshid, 2013). Indeed, earlier biochemical evidence suggested that, in P-gp, the Walker A sequences can approach each other sufficiently closely for a native and/or engineered cysteine in each motif to form a disulfide bond, and thereby inhibit ATP hydrolysis (Loo and Clarke, 2000; Urbatsch et al., 2001). But P-gp structures (all apo so far) show no evidence of such a "twist" or lateral offset, despite their range of NBD separations (11–35 Å; Aller et al., 2009;

Jin et al., 2012; Ward et al., 2013). On the other hand, crystal structures of closed-apo VcMsbA, apo ABCB10, and apo CmABCB1, as well as a recent single-particle cryo-EM structure of apo TmrAB, covering a range of somewhat smaller NBD separations measured directly across the dimer interface (~4–10 Å), do show Walker A motifs that, to varying degrees, face each other—instead of facing signature sequences—across the dimer interface (Ward et al., 2007; Shintre et al., 2013; Kodan et al., 2014; Kim et al., 2015). Moreover, three additional structures of ABCB10 that have AMPPCP or AMPPNP bound to both NBDs but, surprisingly, inward-facing conformations of their transmembrane domains, also display a range of lateral NBD offsets, and of separations across the NBD dimer interface (6–9 Å; Shintre et al., 2013). The single-particle structure of TmrAB is particularly significant because the substantial lateral offset of its NBDs cannot be attributed to distortion resulting from crystal packing (Kim et al., 2015), and also because TmrAB is a bona fide asymmetric ABC protein like TM287/288 and CFTR. The question arises, therefore, as to whether a closed-channel conformation of CFTR might feature laterally offset NBDs like those of TmrAB. If so, CFTR's ABC signature sequences would be directly exposed to solvent, and that would provide a simple alternative explanation for their rapid accessibility.

However, two findings are inconsistent with CFTR's NBDs being sufficiently laterally offset to appose their two Walker A motifs during any part of the CFTR channel gating cycle. First, bismaleimide bifunctional cross-linkers, spanning 8 or 16 Å, were both able to link target cysteine pairs substituted for NBD2 (head) Walker A S1248 and NBD1 (tail) signature sequence S549 (across the active site interface), and cysteine pairs substituted for NBD1 (head) Walker A S459 and V1379, adjacent to NBD2 (tail) D-loop (across the dead site interface). But neither reagent was able to link NBD2 Walker A S1248 to NBD1 Walker A S459 (or NBD1 signature sequence S549 to NBD2 V1379; Mense et al., 2006). The membrane-permeant bismaleimides were applied to CFTR channels actively opening and closing in intact cells, and hence visiting all physiological gating conformations. These (and other) successful and unsuccessful cross-links are compatible with the head-to-tail arrangement of nucleotide-bound homodimers (as in Fig. 1 F; e.g., Smith et al., 2002; Dawson and Locher 2006, 2007; Ward et al., 2007) as well as with apo or AMPPNP-bound TM287/288 (as in Fig. 1 C; Hohl et al., 2012, 2014), but not with any NBD dimer arrangement in which the two Walker A motifs approach within 16 Å of one another (as seen in the TmrAB cryo-EM structure; Kim et al., 2015). If laterally offset NBD conformations can occur under physiological conditions, perhaps they are rare events. Thus, demonstration of the disulfide bonds between Walker A motifs in P-gp required 10–15-min incubations in copper phenanthroline at 37°C, but were not seen at 20°C (Loo and Clarke, 2000; Urbatsch et al., 2001), and so might have reflected cumulative capture of low probability conformations. Second, lateral offset of NBD dimers sufficient to appose Walker A motifs must directly expose both signature sequences to free solution, as suggested by closed apo MsbA (Ward et al., 2007) and apo TmrAB structures (Kim et al., 2015). Such unobstructed exposure of target cysteines in our CFTR channels ought to have rendered them accessible to even the large MTS-biotin–avidin complex. However, as already noted, in our experiments we observed no modification of Cys549 or Cys1347 by the MTS-biotin–avidin complex, although both targets were readily modified by MTS-biotin (Figs. 8 and 9), and the MTS-biotin–avidin complex could readily modify some accessible cysteine in wild-type CFTR (Fig. S6).

Reconciling separation inferred from accessibility with previous findings

How does our demonstration of NBD separation at both interfacial sites during each gating cycle fit with biochemical (Szabó et al., 1999; Aleksandrov et al., 2002; Basso et al., 2003) and functional (Cotten and Welsh, 1998; Tsai et al., 2009, 2010) evidence that nucleotide remains in contact with the NBD1 head of the dead composite site throughout many gating cycles, and that certain NBD1 head residues appear to maintain interactions with components of the NBD2 tail (Szollosi et al., 2011; Hohl et al., 2012)? First, prolonged retention of ATP in the dead site, despite washes with nucleotide-free solution, need not require the NBD1 head to remain closely associated with the NBD2 tail signature sequence, as in tight NBD dimers, because it occurs even in CFTR from which NBD2 has been deleted (Aleksandrov et al., 2008). Thus, although failure of purified isolated NBD1 to retain ATP implies that some other component of CFTR is involved, that component cannot be NBD2 (Aleksandrov et al., 2008). In wild-type CFTR, the azido-ATP that remains after washing becomes cross-linked to the NBD1 head, not the NBD2 tail (Aleksandrov et al., 2002; Basso et al., 2003). Consistent with these findings on CFTR, in TM287/288 crystallized in the presence of 2.5 mM MgAMPPNP, AMPPNP is found bound to the NBD1 (TM287) head (with an additional bond to the second D-loop residue of NBD2 [TM288]), and yet the closest surface of the signature sequence in the NBD2 (TM288) tail is 7 Å distant (Hohl et al., 2012). Despite that separation, positions of the Walker A and B motifs of TM287 and their interactions with the bound AMPPNP mimic those observed in nucleotide-bound tight dimers of Sav1866 (Dawson and Locher, 2007), implying that those interactions might be little altered by engagement with, and disengagement from, the signature sequence in the TM288 tail.

Although closure of CFTR from open bursts is rate-limited by hydrolysis of ATP in the active site, the timing

of hydrolysis appears sensitive to perturbations in and around the dead site, including mutation of the NBD1 Walker A motif (Powe et al., 2002; Vergani et al., 2003; Csanády et al., 2010, 2013) or NBD2 signature sequence (Tsai et al., 2010; Csanády et al., 2013), or replacement of the ATP bound there with an unnatural nucleotide (Tsai et al., 2010; Csanády et al., 2013). The slow time course of establishment of an effect of unnatural nucleotide, inferred to monitor its arrival in the dead site in place of ATP (referred to as "ligand exchange"), was found to be altered by mutation not only of the NBD1 head but also of the NBD2 tail signature sequence (Tsai et al., 2010). This was interpreted as suggesting that close contact of the NBD1 head with the NBD2 tail signature motif throughout many (≥50) gating cycles is required to sustain the normal prolonged occupancy of the dead site by ATP (Tsai et al., 2009, 2010). Similarly, unaltered energetic coupling between an NBD1 Walker A residue and each of three NBD2 tail residues, whether a CFTR channel is open or closed, was interpreted to suggest their sustained interaction across the NBD dimer interface (Szollosi et al., 2011). However, the equivalent residues to one of those pairs is now seen in TM287/288 to link the NBD1 Walker A and NBD2 D-loop in both the AMPPNP-bound and the apo structures (Hohl et al., 2012, 2014), so providing a reasonable alternative explanation for at least some of the mutant cycle data (Szollosi et al., 2011). Moreover, further energetic study of the dead site, including analysis of an NBD2 signature-sequence mutant at position H1348, adjacent to our target position S1347, demonstrates structural changes within the dead site between open- and closed-channel conformations (Csanády et al., 2013). Whether the influence of NBD2 signature-sequence mutations on nucleotide occupancy of the dead site (Tsai et al., 2009, 2010) might now be explained by indirect interactions propagated from the NBD2 signature sequence to the adjacent NBD2 D-loop, and hence directly to both the NBD1 Walker A motif and the tightly bound nucleotide (Hohl et al., 2012), remains to be established. Regardless, the present demonstration of near simultaneous accessibility of cysteines substituted for both signature-sequence serines as a CFTR channel closes during each gating, and catalytic, cycle provides direct evidence that NBD1 and NBD2 separate all along the dimer interface, even if a subset of NBD1 and NBD2 residues maintain contact through NBD2 D-loop and NBD1 Walker A interactions.

Implications of functional observations on modified channels

What can we learn about the function of CFTR, and perhaps of other ABC proteins, from the behavior of the channels after their stoichiometric modification by MTS reagents? The fact that ATP-dependent current persisted after MTS modification means that CFTR channels continued to open and close, despite the presence of an ∼8-Å long, 6-Å wide adduct covalently attached to one or other signature sequence. This is remarkable because the side chain at the substituted position normally H-bonds to the ATP γ phosphate in the nucleotide-bound tight dimer (e.g., Smith et al., 2002; Verdon et al., 2003; Dawson and Locher, 2006; Oldham and Chen, 2011b). Insofar as the current decay on sudden ATP withdrawal reports the ensemble time course of channel closing, its time constant provides an estimate of mean open burst duration. The similarity of the current decay time constants on ATP washout before and after modification (Figs. 3 E, 5 E, and S6 E) implies that the modification left the timing of channel closing unaltered and, hence, that residual current amplitudes reflect the severity of impairment of channel opening. The residual current after MTSACE modification of S549C was ∼18%, and of S1347C was ∼20%, of control current, indicating that the neutral MTS adduct, whether in the active or dead composite site, made channel opening about fivefold less probable (assuming control P_o of ∼0.1 for both S549C and S1347C; compare Csanády et al., 2000; Vergani et al., 2003; Fig. S1 in Mense et al., 2006). Presumably, the presence of the adduct at either signature sequence sterically impedes formation of the tight NBD1–NBD2 dimer after ATP has bound at both Walker A motifs. In contrast, the residual current after $MTSET^+$ modification varied with position along the dimer interface, and was ∼4% of control with the adduct at S549C (Fig. 4), 10–20% at A1374C (Fig. 11), ∼20% at S605C (Fig. 10), and ∼40% at S1347C (Fig. 6). This reveals a gradient of influence of the positively charged adduct to lower the frequency of channel opening, from very severe (∼30-fold) at the catalytically active site, to less severe (∼5–11-fold) near the middle of the interface, to weak (two- to threefold) at the dead site. Interestingly, relative to the effect of the similarly sized neutral adduct, the positive charge itself further impaired channel opening when introduced into the catalytic site, but mildly enhanced opening rate when introduced into the dead site. Interpretation of this observation will require improved understanding of electrostatic contributions to formation and disruption of NBD dimers (e.g., Smith et al., 2002).

Perhaps more remarkable is the inference, from the similarity of the current decay time courses upon ATP washout before and after modification, that once a modified channel has opened—presumably by eventual assembly of a tight NBD dimer—the timing of channel closure is unaltered. In other words, the closing process appears little affected by the presence of either the charged or neutral adduct in the dead site, or by the neutral adduct in the catalytic site. Closure of these cysteine-depleted channels containing a target cysteine is slowed at least an order of magnitude after the addition of the K1250R mutation (Figs. 7 and S4), arguing that closure of the unmodified channels, like that of wild-type CFTR, is normally rate-limited by hydrolysis of

the ATP bound in the active site between NBD2 Walker A and NBD1 LSGGQ sequences. One interpretation of the unaltered timing of S549C channel closure after MTSACE modification is that ATP hydrolysis at the active site still controls closing, even though the modified channels contain a 6-Å-thick neutral adduct extending 8 Å from the position of the signature-sequence serine that, when present, contacts the γ phosphate of the hydrolyzed ATP. The same interpretation would hold for the charged or neutral adducts in the dead site (as well as for the charged adduct mid interface; Fig. 10). This would all imply that the composite sites are flexible enough to accommodate both a tethered adduct and MgATP in either site, without perturbing hydrolysis of the ATP in the active site. An extreme alternative possibility is that the adducts do interfere with hydrolysis of the ATP, delaying it, but that an adduct in either site, or in mid interface, also destabilizes the dimer interface such that the NBDs separate, causing channel closure, at about the same time as when those events are triggered by ATP hydrolysis in the unmodified channels.

Although the most parsimonious interpretation would be that none of these adducts alters the timing of ATP hydrolysis, and hence of hydrolysis-triggered channel closure, one observation suggests that the neutral adduct in the dead site might somewhat destabilize the ATP-bound prehydrolytic dimer. That observation is the apparent absence of residual current after MTSACE modification of S1374C-K1250R channels (Fig. 7 B) that are believed to close by nonhydrolytic dissociation of the NBD dimer (Vergani et al., 2005; Csanády et al., 2006, 2010), in contrast to the ∼20% residual current after MTSACE observed (Figs. 5 B and 6 B) for S1347C channels that are closed by ATP hydrolysis. Opening rate of K1250R CFTR channels is maximal at 3 mM ATP (half-maximal [ATP] is ∼150 µM; Szollosi et al., 2010) and comparable to that of wild-type CFTR (within a factor of 2 given the 10-fold longer open bursts, and P_o of ∼0.5, for K1250R; Vergani et al., 2005; Csanády et al., 2006, 2010; Szollosi et al., 2010). If the MTSACE adduct in the dead site influenced only channel opening, and exerted a similar approximate fivefold slowing effect on the opening of modified S1374C-K1250R channels as estimated above for modified S1347C channels, the residual current amplitude (percentage of control) of S1374C-K1250R ought to have been no smaller than that of S1347; in fact, it should be larger (≥30%) because of their expected higher P_o that results from slower closing. The lack of measurable (≥5%) residual current in modified S1347C-K1250R channels, therefore, implies that the MTSACE adduct in the dead site exerted an additional effect, acceleration of nonhydrolytic closure; i.e., an increased rate k_{-1} of the step $O_1 \rightarrow C$, the reversal of CFTR channel opening in the gating cycle $C \rightleftharpoons O_1 \rightarrow O_2 \rightarrow C$ (Csanády et al., 2010). These combined effects of the neutral adduct, apparent severalfold slowing of opening ($C \rightarrow O_1$; see above) and inferred severalfold speeding of nonhydrolytic closure ($O_1 \rightarrow C$), could together explain the absence of measurable residual current of MTSACE-modified S1347C-K1250R channels. Assuming the K1250R mutation makes the rate k_1 of the $O_1 \rightarrow O_2$ ATP hydrolysis step zero, the ATP washout time constant for unmodified S1347C-K1250R channels (Fig. 7 C) suggests that k_{-1} is $\sim 0.06\ s^{-1}$, reflecting the considerable stability of the prehydrolytic NBD dimer. The ATP washout time constant for unmodified S1347C channels (Fig. 5 C) suggests that k_1, which rate-limits hydrolytic closure, is $\sim 1\ s^{-1}$ (k_2, the rate of post-hydrolytic dimer dissociation, $O_2 \rightarrow C$, is ∼11-fold faster than k_1; Csanády et al., 2010). Because k_1 is more than an order of magnitude larger than k_{-1}, even the inferred severalfold increase of k_{-1} caused by the neutral adduct would be expected to little affect the hydrolysis-mediated closing rate of modified S1347C channels; and even larger destabilizing effects on k_{-1} might be masked by any tendency of the adducts to also delay ATP hydrolysis, i.e., to diminish k_1. Single-channel recordings could provide further insights into these considerations.

Finally, if the MTS adduct does destabilize the prehydrolytic dimer once S1347C-K1250R CFTR channels are modified, as the above analysis suggests, then our conclusion of strict state dependence of modification is further strengthened, particularly for nonhydrolytic channels. Otherwise, modification in the presence of ATP while S1347C-K1250R channels were open should have caused current to decay more rapidly than upon ATP washout before modification, contrary to observation (Figs. 7 and S4). This failure to modify either signature-sequence cysteine in a nonhydrolytic channel until it is closed by dimer separation is satisfactorily explained by the expected presence of two intact ATP molecules in the tight NBD dimer interface as long as the channel remains open, shielding both cysteines. But what about CFTR channels that close by ATP hydrolysis? Locking of CFTR channels into prolonged open bursts by orthovanadate or beryllium fluoride (Baukrowitz et al., 1994; Gunderson and Kopito, 1994), like stable trapping of the hydrolytic transition state in other ABC proteins (Urbatsch et al., 1995; Fetsch and Davidson, 2002; Janas et al., 2003; Oldham and Chen, 2011b; Zutz et al., 2011), demonstrates that the severed γ phosphate can exit, and a phosphate analogue can enter, the catalytic site without disruption of the tight NBD dimer. However, even if the phosphate exit route were wide enough for MTS reagents to reach and modify signature-sequence target cysteines while channels were still open, our conclusions would remain unaltered. Because no phosphate is released from the dead site, MTS access to S1347C requires dimer separation and hence channel closure, as for K1250R mutants. Also, as ATP hydrolysis does not occur at the active site until after >90% of the open burst duration has passed (Csanády et al., 2010),

any MTS modification of open S549C channels after phosphate release would be limited to <10% of the open time, i.e., <1% of the gating cycle for P_o of ~0.1. The two orders of magnitude greater opportunity for MTS modification after NBD dimer separation and channel closure amply justifies the conclusion of strong, and likely exclusive, preference for closed-state modification also for hydrolytic CFTR channels.

We thank Martin Mense for carrying out preliminary experiments, László Csanády for helpful discussion, Peter Hoff for preparing oocytes, and Nazim Fataliev for molecular biological support.

This work was supported by National Institutes of Health grant DK51767 to D.C. Gadsby.

The authors declare no competing financial interests.

Merritt C. Maduke served as editor.

Submitted: 14 December 2014
Accepted: 27 February 2015

REFERENCES

Aleksandrov, L., A.A. Aleksandrov, X.B. Chang, and J.R. Riordan. 2002. The first nucleotide binding domain of cystic fibrosis transmembrane conductance regulator is a site of stable nucleotide interaction, whereas the second is a site of rapid turnover. *J. Biol. Chem.* 277:15419–15425. http://dx.doi.org/10.1074/jbc.M111713200

Aleksandrov, L., A. Aleksandrov, and J.R. Riordan. 2008. Mg^{2+}-dependent ATP occlusion at the first nucleotide-binding domain (NBD1) of CFTR does not require the second (NBD2). *Biochem. J.* 416:129–136. http://dx.doi.org/10.1042/BJ20081068

Aller, S.G., J. Yu, A. Ward, Y. Weng, S. Chittaboina, R. Zhuo, P.M. Harrell, Y.T. Trinh, Q. Zhang, I.L. Urbatsch, and G. Chang. 2009. Structure of P-glycoprotein reveals a molecular basis for poly-specific drug binding. *Science.* 323:1718–1722. http://dx.doi.org/10.1126/science.1168750

Bai, Y., M. Li, and T.C. Hwang. 2010. Dual roles of the sixth transmembrane segment of the CFTR chloride channel in gating and permeation. *J. Gen. Physiol.* 136:293–309. http://dx.doi.org/10.1085/jgp.201010480

Basso, C., P. Vergani, A.C. Nairn, and D.C. Gadsby. 2003. Prolonged nonhydrolytic interaction of nucleotide with CFTR's NH_2-terminal nucleotide binding domain and its role in channel gating. *J. Gen. Physiol.* 122:333–348. http://dx.doi.org/10.1085/jgp.200308798

Baukrowitz, T., T.C. Hwang, A.C. Nairn, and D.C. Gadsby. 1994. Coupling of CFTR Cl^- channel gating to an ATP hydrolysis cycle. *Neuron.* 12:473–482. http://dx.doi.org/10.1016/0896-6273(94)90206-2

Boël, G., P.C. Smith, W. Ning, M.T. Englander, B. Chen, Y. Hashem, A.J. Testa, J.J. Fischer, H.J. Wieden, J. Frank, et al. 2014. The ABC-F protein EttA gates ribosome entry into the translation elongation cycle. *Nat. Struct. Mol. Biol.* 21:143–151. http://dx.doi.org/10.1038/nsmb.2740

Cai, Z., T.S. Scott-Ward, and D.N. Sheppard. 2003. Voltage-dependent gating of the cystic fibrosis transmembrane conductance regulator Cl^- channel. *J. Gen. Physiol.* 122:605–620. http://dx.doi.org/10.1085/jgp.200308921

Carson, M.R., S.M. Travis, and M.J. Welsh. 1995. The two nucleotide-binding domains of cystic fibrosis transmembrane conductance regulator (CFTR) have distinct functions in controlling channel activity. *J. Biol. Chem.* 270:1711–1717. http://dx.doi.org/10.1074/jbc.270.4.1711

Chan, K.W., L. Csanády, D. Seto-Young, A.C. Nairn, and D.C. Gadsby. 2000. Severed molecules functionally define the boundaries of the cystic fibrosis transmembrane conductance regulator's Nh_2-terminal nucleotide binding domain. *J. Gen. Physiol.* 116:163–180. http://dx.doi.org/10.1085/jgp.116.2.163

Chen, T.Y., and T.C. Hwang. 2008. CLC-0 and CFTR: Chloride channels evolved from transporters. *Physiol. Rev.* 88:351–387. http://dx.doi.org/10.1152/physrev.00058.2006

Chen, J., G. Lu, J. Lin, A.L. Davidson, and F.A. Quiocho. 2003. A tweezers-like motion of the ATP-binding cassette dimer in an ABC transport cycle. *Mol. Cell.* 12:651–661. http://dx.doi.org/10.1016/j.molcel.2003.08.004

Cotten, J.F., and M.J. Welsh. 1997. Covalent modification of the regulatory domain irreversibly stimulates cystic fibrosis transmembrane conductance regulator. *J. Biol. Chem.* 272:25617–25622. http://dx.doi.org/10.1074/jbc.272.41.25617

Cotten, J.F., and M.J. Welsh. 1998. Covalent modification of the nucleotide binding domains of cystic fibrosis transmembrane conductance regulator. *J. Biol. Chem.* 273:31873–31879. http://dx.doi.org/10.1074/jbc.273.48.31873

Csanády, L., K.W. Chan, D. Seto-Young, D.C. Kopsco, A.C. Nairn, and D.C. Gadsby. 2000. Severed channels probe regulation of gating of cystic fibrosis transmembrane conductance regulator by its cytoplasmic domains. *J. Gen. Physiol.* 116:477–500. http://dx.doi.org/10.1085/jgp.116.3.477

Csanády, L., A.C. Nairn, and D.C. Gadsby. 2006. Thermodynamics of CFTR channel gating: A spreading conformational change initiates an irreversible gating cycle. *J. Gen. Physiol.* 128:523–533. http://dx.doi.org/10.1085/jgp.200609558

Csanády, L., P. Vergani, and D.C. Gadsby. 2010. Strict coupling between CFTR's catalytic cycle and gating of its Cl^- ion pore revealed by distributions of open channel burst durations. *Proc. Natl. Acad. Sci. USA.* 107:1241–1246. http://dx.doi.org/10.1073/pnas.0911061107

Csanády, L., C. Mihályi, A. Szollosi, B. Töröcsik, and P. Vergani. 2013. Conformational changes in the catalytically inactive nucleotide-binding site of CFTR. *J. Gen. Physiol.* 142:61–73. http://dx.doi.org/10.1085/jgp.201210954

Cui, L., L. Aleksandrov, Y.X. Hou, M. Gentzsch, J.H. Chen, J.R. Riordan, and A.A. Aleksandrov. 2006. The role of cystic fibrosis transmembrane conductance regulator phenylalanine 508 side chain in ion channel gating. *J. Physiol.* 572:347–358. http://dx.doi.org/10.1113/jphysiol.2005.099457

Davidson, A.L., E. Dassa, C. Orelle, and J. Chen. 2008. Structure, function, and evolution of bacterial ATP-binding cassette systems. *Microbiol. Mol. Biol. Rev.* 72:317–364. http://dx.doi.org/10.1128/MMBR.00031-07

Dawson, R.J., and K.P. Locher. 2006. Structure of a bacterial multidrug ABC transporter. *Nature.* 443:180–185. http://dx.doi.org/10.1038/nature05155

Dawson, R.J., and K.P. Locher. 2007. Structure of the multidrug ABC transporter Sav1866 from *Staphylococcus aureus* in complex with AMP-PNP. *FEBS Lett.* 581:935–938. http://dx.doi.org/10.1016/j.febslet.2007.01.073

Fetsch, E.E., and A.L. Davidson. 2002. Vanadate-catalyzed photocleavage of the signature motif of an ATP-binding cassette (ABC) transporter. *Proc. Natl. Acad. Sci. USA.* 99:9685–9690. http://dx.doi.org/10.1073/pnas.152204499

Gadsby, D.C., P. Vergani, and L. Csanády. 2006. The ABC protein turned chloride channel whose failure causes cystic fibrosis. *Nature.* 440:477–483. http://dx.doi.org/10.1038/nature04712

Gao, M., H.R. Cui, D.W. Loe, C.E. Grant, K.C. Almquist, S.P. Cole, and R.G. Deeley. 2000. Comparison of the functional characteristics of the nucleotide binding domains of multidrug resistance protein 1. *J. Biol. Chem.* 275:13098–13108. http://dx.doi.org/10.1074/jbc.275.17.13098

Gunderson, K.L., and R.R. Kopito. 1994. Effects of pyrophosphate and nucleotide analogs suggest a role for ATP hydrolysis in cystic

fibrosis transmembrane regulator channel gating. *J. Biol. Chem.* 269:19349–19353.

Gunderson, K.L., and R.R. Kopito. 1995. Conformational states of CFTR associated with channel gating: The role ATP binding and hydrolysis. *Cell.* 82:231–239. http://dx.doi.org/10.1016/0092-8674(95)90310-0

Hohl, M., C. Briand, M.G. Grütter, and M.A. Seeger. 2012. Crystal structure of a heterodimeric ABC transporter in its inward-facing conformation. *Nat. Struct. Mol. Biol.* 19:395–402. http://dx.doi.org/10.1038/nsmb.2267

Hohl, M., L.M. Hürlimann, S. Böhm, J. Schöppe, M.G. Grütter, E. Bordignon, and M.A. Seeger. 2014. Structural basis for allosteric cross-talk between the asymmetric nucleotide binding sites of a heterodimeric ABC exporter. *Proc. Natl. Acad. Sci. USA.* 111:11025–11030. http://dx.doi.org/10.1073/pnas.1400485111

Hopfner, K.P., and J.A. Tainer. 2003. Rad50/SMC proteins and ABC transporters: unifying concepts from high-resolution structures. *Curr. Opin. Struct. Biol.* 13:249–255. http://dx.doi.org/10.1016/S0959-440X(03)00037-X

Hopfner, K.P., A. Karcher, D.S. Shin, L. Craig, L.M. Arthur, J.P. Carney, and J.A. Tainer. 2000. Structural biology of Rad50 ATPase: ATP-driven conformational control in DNA double-strand break repair and the ABC-ATPase superfamily. *Cell.* 101:789–800. http://dx.doi.org/10.1016/S0092-8674(00)80890-9

Hou, Y., L. Cui, J.R. Riordan, and X. Chang. 2000. Allosteric interactions between the two non-equivalent nucleotide binding domains of multidrug resistance protein MRP1. *J. Biol. Chem.* 275:20280–20287. http://dx.doi.org/10.1074/jbc.M001109200

Hung, L.W., I.X. Wang, K. Nikaido, P.Q. Liu, G.F. Ames, and S.H. Kim. 1998. Crystal structure of the ATP-binding subunit of an ABC transporter. *Nature.* 396:703–707. http://dx.doi.org/10.1038/25393

Janas, E., M. Hofacker, M. Chen, S. Gompf, C. van der Does, and R. Tampé. 2003. The ATP hydrolysis cycle of the nucleotide-binding domain of the mitochondrial ATP-binding cassette transporter Mdl1p. *J. Biol. Chem.* 278:26862–26869. http://dx.doi.org/10.1074/jbc.M301227200

Jin, M.S., M.L. Oldham, Q. Zhang, and J. Chen. 2012. Crystal structure of the multidrug transporter P-glycoprotein from *Caenorhabditis elegans*. *Nature.* 490:566–569. http://dx.doi.org/10.1038/nature11448

Karlin, A., and M.H. Akabas. 1998. Substituted-cysteine accessibility method. *Methods Enzymol.* 293:123–145. http://dx.doi.org/10.1016/S0076-6879(98)93011-7

Khare, D., M.L. Oldham, C. Orelle, A.L. Davidson, and J. Chen. 2009. Alternating access in maltose transporter mediated by rigid-body rotations. *Mol. Cell.* 33:528–536. http://dx.doi.org/10.1016/j.molcel.2009.01.035

Kim, J., S. Wu, T.M. Tomasiak, C. Mergel, M.B. Winter, S.B. Stiller, Y. Robles-Colmanares, R.M. Stroud, R. Tampé, C.S. Craik, and Y. Cheng. 2015. Subnanometre-resolution electron cryomicroscopy structure of a heterodimeric ABC exporter. *Nature.* 517:396–400. http://dx.doi.org/10.1038/nature13872

Kodan, A., T. Yamaguchi, T. Nakatsu, K. Sakiyama, C.J. Hipolito, A. Fujioka, R. Hirokane, K. Ikeguchi, B. Watanabe, J. Hiratake, et al. 2014. Structural basis for gating mechanisms of a eukaryotic P-glycoprotein homolog. *Proc. Natl. Acad. Sci. USA.* 111:4049–4054. http://dx.doi.org/10.1073/pnas.1321562111

Kuruma, A., and H.C. Hartzell. 2000. Bimodal control of a Ca^{2+}-activated Cl^- channel by different Ca^{2+} signals. *J. Gen. Physiol.* 115:59–80. http://dx.doi.org/10.1085/jgp.115.1.59

Lamers, M.H., H.H. Winterwerp, and T.K. Sixma. 2003. The alternating ATPase domains of MutS control DNA mismatch repair. *EMBO J.* 22:746–756. http://dx.doi.org/10.1093/emboj/cdg064

Lee, J.Y., J.G. Yang, D. Zhitnitsky, O. Lewinson, and D.C. Rees. 2014. Structural basis for heavy metal detoxification by an Atm1-type ABC exporter. *Science.* 343:1133–1136. http://dx.doi.org/10.1126/science.1246489

Lerner-Marmarosh, N., K. Gimi, I.L. Urbatsch, P. Gros, and A.E. Senior. 1999. Large scale purification of detergent-soluble P-glycoprotein from *Pichia pastoris* cells and characterization of nucleotide binding properties of wild-type, Walker A, and Walker B mutant proteins. *J. Biol. Chem.* 274:34711–34718. http://dx.doi.org/10.1074/jbc.274.49.34711

Lewis, H.A., S.G. Buchanan, S.K. Burley, K. Conners, M. Dickey, M. Dorwart, R. Fowler, X. Gao, W.B. Guggino, W.A. Hendrickson, et al. 2004. Structure of nucleotide-binding domain 1 of the cystic fibrosis transmembrane conductance regulator. *EMBO J.* 23:282–293.

Li, C.H., Y.X. Yang, J.G. Su, B. Liu, J.J. Tan, X.Y. Zhang, and C.X. Wang. 2014. Allosteric transitions of the maltose transporter studied by an elastic network model. *Biopolymers.* 101:758–768. http://dx.doi.org/10.1002/bip.22455

Loo, T.W., and D.M. Clarke. 2000. Drug-stimulated ATPase activity of human P-glycoprotein is blocked by disulfide cross-linking between the nucleotide-binding sites. *J. Biol. Chem.* 275:19435–19438. http://dx.doi.org/10.1074/jbc.C000222200

Lubelski, J., A. de Jong, R. van Merkerk, H. Agustiandari, O.P. Kuipers, J. Kok, and A.J. Driessen. 2006. LmrCD is a major multidrug resistance transporter in *Lactococcus lactis*. *Mol. Microbiol.* 61:771–781. http://dx.doi.org/10.1111/j.1365-2958.2006.05267.x

Matsuo, M., N. Kioka, T. Amachi, and K. Ueda. 1999. ATP binding properties of the nucleotide-binding folds of SUR1. *J. Biol. Chem.* 274:37479–37482. http://dx.doi.org/10.1074/jbc.274.52.37479

Mense, M., P. Vergani, D.M. White, G. Altberg, A.C. Nairn, and D.C. Gadsby. 2006. In vivo phosphorylation of CFTR promotes formation of a nucleotide-binding domain heterodimer. *EMBO J.* 25:4728–4739. http://dx.doi.org/10.1038/sj.emboj.7601373

Moody, J.E., L. Millen, D. Binns, J.F. Hunt, and P.J. Thomas. 2002. Cooperative, ATP-dependent association of the nucleotide binding cassettes during the catalytic cycle of ATP-binding cassette transporters. *J. Biol. Chem.* 277:21111–21114. http://dx.doi.org/10.1074/jbc.C200228200

Moradi, M., and E. Tajkhorshid. 2013. Mechanistic picture for conformational transition of a membrane transporter at atomic resolution. *Proc. Natl. Acad. Sci. USA.* 110:18916–18921. http://dx.doi.org/10.1073/pnas.1313202110

Nagata, K., M. Nishitani, M. Matsuo, N. Kioka, T. Amachi, and K. Ueda. 2000. Nonequivalent nucleotide trapping in the two nucleotide binding folds of the human multidrug resistance protein MRP1. *J. Biol. Chem.* 275:17626–17630. http://dx.doi.org/10.1074/jbc.M000792200

Oldham, M.L., and J. Chen. 2011a. Crystal structure of the maltose transporter in a pretranslocation intermediate state. *Science.* 332:1202–1205. http://dx.doi.org/10.1126/science.1200767

Oldham, M.L., and J. Chen. 2011b. Snapshots of the maltose transporter during ATP hydrolysis. *Proc. Natl. Acad. Sci. USA.* 108:15152–15156. http://dx.doi.org/10.1073/pnas.1108858108

Powe, A.C., Jr., L. Al-Nakkash, M. Li, and T.C. Hwang. 2002. Mutation of Walker-A lysine 464 in cystic fibrosis transmembrane conductance regulator reveals functional interaction between its nucleotide-binding domains. *J. Physiol.* 539:333–346. http://dx.doi.org/10.1113/jphysiol.2001.013162

Procko, E., I. Ferrin-O'Connell, S.L. Ng, and R. Gaudet. 2006. Distinct structural and functional properties of the ATPase sites in an asymmetric ABC transporter. *Mol. Cell.* 24:51–62. http://dx.doi.org/10.1016/j.molcel.2006.07.034

Ramjeesingh, M., C. Li, E. Garami, L.J. Huan, K. Galley, Y. Wang, and C.E. Bear. 1999. Walker mutations reveal loose relationship between catalytic and channel-gating activities of purified CFTR (cystic fibrosis transmembrane conductance regulator). *Biochemistry.* 38:1463–1468. http://dx.doi.org/10.1021/bi982243y

Rees, D.C., E. Johnson, and O. Lewinson. 2009. ABC transporters: the power to change. *Nat. Rev. Mol. Cell Biol.* 10:218–227. http://dx.doi.org/10.1038/nrm2646

Senior, A.E., M.K. al-Shawi, and I.L. Urbatsch. 1995. The catalytic cycle of P-glycoprotein. *FEBS Lett.* 377:285–289. http://dx.doi.org/10.1016/0014-5793(95)01345-8

Shintre, C.A., A.C. Pike, Q. Li, J.I. Kim, A.J. Barr, S. Goubin, L. Shrestha, J. Yang, G. Berridge, J. Ross, et al. 2013. Structures of ABCB10, a human ATP-binding cassette transporter in apo- and nucleotide-bound states. *Proc. Natl. Acad. Sci. USA.* 110:9710–9715.

Siarheyeva, A., R. Liu, and F.J. Sharom. 2010. Characterization of an asymmetric occluded state of P-glycoprotein with two bound nucleotides: Implications for catalysis. *J. Biol. Chem.* 285:7575–7586. http://dx.doi.org/10.1074/jbc.M109.047290

Smith, P.C., N. Karpowich, L. Millen, J.E. Moody, J. Rosen, P.J. Thomas, and J.F. Hunt. 2002. ATP binding to the motor domain from an ABC transporter drives formation of a nucleotide sandwich dimer. *Mol. Cell.* 10:139–149. http://dx.doi.org/10.1016/S1097-2765(02)00576-2

Srinivasan, V., A.J. Pierik, and R. Lill. 2014. Crystal structures of nucleotide-free and glutathione-bound mitochondrial ABC transporter Atm1. *Science.* 343:1137–1140. http://dx.doi.org/10.1126/science.1246729

Szabó, K., G. Szakács, T. Hegeds, and B. Sarkadi. 1999. Nucleotide occlusion in the human cystic fibrosis transmembrane conductance regulator. Different patterns in the two nucleotide binding domains. *J. Biol. Chem.* 274:12209–12212. http://dx.doi.org/10.1074/jbc.274.18.12209

Szollosi, A., P. Vergani, and L. Csanády. 2010. Involvement of F1296 and N1303 of CFTR in induced-fit conformational change in response to ATP binding at NBD2. *J. Gen. Physiol.* 136:407–423.

Szollosi, A., D.R. Muallem, L. Csanády, and P. Vergani. 2011. Mutant cycles at CFTR's non-canonical ATP-binding site support little interface separation during gating. *J. Gen. Physiol.* 137:549–562. http://dx.doi.org/10.1085/jgp.201110608

Tombline, G., and A.E. Senior. 2005. The occluded nucleotide conformation of p-glycoprotein. *J. Bioenerg. Biomembr.* 37:497–500. http://dx.doi.org/10.1007/s10863-005-9498-4

Tsai, M.F., H. Shimizu, Y. Sohma, M. Li, and T.C. Hwang. 2009. State-dependent modulation of CFTR gating by pyrophosphate. *J. Gen. Physiol.* 133:405–419. http://dx.doi.org/10.1085/jgp.200810186

Tsai, M.F., M. Li, and T.C. Hwang. 2010. Stable ATP binding mediated by a partial NBD dimer of the CFTR chloride channel. *J. Gen. Physiol.* 135:399–414. http://dx.doi.org/10.1085/jgp.201010399

Urbatsch, I.L., B. Sankaran, S. Bhagat, and A.E. Senior. 1995. Both P-glycoprotein nucleotide-binding sites are catalytically active. *J. Biol. Chem.* 270:26956–26961. http://dx.doi.org/10.1074/jbc.270.45.26956

Urbatsch, I.L., K. Gimi, S. Wilke-Mounts, N. Lerner-Marmarosh, M.E. Rousseau, P. Gros, and A.E. Senior. 2001. Cysteines 431 and 1074 are responsible for inhibitory disulfide cross-linking between the two nucleotide-binding sites in human P-glycoprotein. *J. Biol. Chem.* 276:26980–26987. http://dx.doi.org/10.1074/jbc.M010829200

Verdon, G., S.V. Albers, N. van Oosterwijk, B.W. Dijkstra, A.J. Driessen, and A.M. Thunnissen. 2003. Formation of the productive ATP-Mg^{2+}-bound dimer of GlcV, an ABC-ATPase from *Sulfolobus solfataricus*. *J. Mol. Biol.* 334:255–267. http://dx.doi.org/10.1016/j.jmb.2003.08.065

Vergani, P., A.C. Nairn, and D.C. Gadsby. 2003. On the mechanism of MgATP-dependent gating of CFTR Cl^- channels. *J. Gen. Physiol.* 121:17–36. http://dx.doi.org/10.1085/jgp.20028673

Vergani, P., S.W. Lockless, A.C. Nairn, and D.C. Gadsby. 2005. CFTR channel opening by ATP-driven tight dimerization of its nucleotide-binding domains. *Nature.* 433:876–880. http://dx.doi.org/10.1038/nature03313

Ward, A., C.L. Reyes, J. Yu, C.B. Roth, and G. Chang. 2007. Flexibility in the ABC transporter MsbA: Alternating access with a twist. *Proc. Natl. Acad. Sci. USA.* 104:19005–19010. http://dx.doi.org/10.1073/pnas.0709388104

Ward, A.B., P. Szewczyk, V. Grimard, C.W. Lee, L. Martinez, R. Doshi, A. Caya, M. Villaluz, E. Pardon, C. Cregger, et al. 2013. Structures of P-glycoprotein reveal its conformational flexibility and an epitope on the nucleotide-binding domain. *Proc. Natl. Acad. Sci. USA.* 110:13386–13391. http://dx.doi.org/10.1073/pnas.1309275110

Zaitseva, J., S. Jenewein, A. Wiedenmann, H. Benabdelhak, I.B. Holland, and L. Schmitt. 2005. Functional characterization and ATP-induced dimerization of the isolated ABC-domain of the haemolysin B transporter. *Biochemistry.* 44:9680–9690.

Zutz, A., J. Hoffmann, U.A. Hellmich, C. Glaubitz, B. Ludwig, B. Brutschy, and R. Tampé. 2011. Asymmetric ATP hydrolysis cycle of the heterodimeric multidrug ABC transport complex TmrAB from *Thermus thermophilus*. *J. Biol. Chem.* 286:7104–7115. http://dx.doi.org/10.1074/jbc.M110.201178